

1 **The apicoplast link to fever-survival and artemisinin-resistance in the malaria**  
2 **parasite**

3

4 Min Zhang<sup>a,1</sup>, Chengqi Wang<sup>a,1</sup>, Jenna Oberstaller<sup>a,1</sup>, Phaedra Thomas<sup>a</sup>, Thomas D.  
5 Otto<sup>b,c</sup>, Debora Casandra<sup>a</sup>, Sandhya Boyapalle<sup>a</sup>, Swamy R. Adapa<sup>a</sup>, Shulin Xu<sup>a</sup>, Katrina  
6 Button-Simons<sup>d</sup>, Matthew Mayho<sup>b</sup>, Julian C. Rayner<sup>b,e</sup>, Michael T. Ferdig<sup>e</sup>, Rays H. Y.  
7 Jiang<sup>a</sup>, John H. Adams<sup>a,2</sup>

8

9 <sup>a</sup>Center for Global Health and Infectious Diseases Research and USF Genomics  
10 Program, College of Public Health, University of South Florida, 3720 Spectrum Blvd,  
11 Suite 404, Tampa, Florida 33612, USA

12

13 <sup>b</sup>Wellcome Sanger Institute, Wellcome Genome Campus, Hinxton Cambridgeshire,  
14 CB10 1SA United Kingdom

15

16 <sup>c</sup>Institute of Infection, Immunity and Inflammation, MVLS, University of Glasgow,  
17 Glasgow G12 8TA United Kingdom

18

19 <sup>d</sup>Eck Institute for Global Health, Department of Biological Sciences, University of Notre  
20 Dame, Notre Dame, IN 46556

21

22 <sup>e</sup>Cambridge Institute for Medical Research, University of Cambridge, Cambridge  
23 Biomedical Campus, The Keith Peters Building, Hills Road, Cambridge, Cambridgeshire,  
24 CB2 0XY United Kingdom

25

26 <sup>1</sup> M.Z., C.W. and J.O. contributed equally to this work.

27 <sup>2</sup>To whom correspondence should be addressed. Email: [ja2@usf.edu](mailto:ja2@usf.edu)

## 28 **ABSTRACT**

29 **Background:** The emergence and spread of *Plasmodium falciparum* parasites resistant  
30 to front-line antimalarial artemisinin-combination therapies (ACT) threatens to erase the  
31 considerable gains against the disease of the last decade. We developed a new large-  
32 scale phenotypic screening pipeline and used it to carry out the first large-scale forward-  
33 genetic phenotype screen in *P. falciparum* to identify genes that allow parasites to  
34 survive febrile temperatures.

35 **Results:** Screening identified more than 200 *P. falciparum* mutants with differential  
36 responses to increased temperature. These mutants were more likely to be sensitive to  
37 artemisinin derivatives as well as to heightened oxidative stress. Major processes critical  
38 for *P. falciparum* tolerance to febrile temperatures and artemisinin included highly  
39 essential, conserved pathways associated with protein-folding, heat-shock and  
40 proteasome-mediated degradation, and unexpectedly, isoprenoid biosynthesis, which  
41 originated from the ancestral genome of the parasite's algal endosymbiont-derived  
42 plastid, the apicoplast. Apicoplast-targeted genes in general were up-regulated in  
43 response to heat shock, as were other *Plasmodium* genes with orthologs in plant and  
44 algal genomes.

45 **Conclusions:** *Plasmodium falciparum* parasites appear to exploit their innate febrile-  
46 response mechanisms to mediate resistance to artemisinin. Both responses depend on  
47 endosymbiotic cyanobacterium-related ancestral genes in the parasite's genome,  
48 suggesting a link to the evolutionary origins of *Plasmodium* parasites in free-living  
49 ancestors.

50

51 **Running title:** Plastid metabolism enables malaria parasites to survive fever and  
52 artemisinin

53

54 **Key words:** genome-wide phenotypic screens, *piggyBac*, QIseq, heat shock, growth  
55 fitness, transposon-mediated mutagenesis, phenotypic functional profiling

56

## 57 INTRODUCTION

58 Malaria remains a leading infectious disease causing >200 million clinical cases and a  
59 half-million deaths every year. *Plasmodium falciparum* is the deadliest malaria parasite  
60 by far, with growing parasite resistance to front-line antimalarial artemisinin-combination  
61 therapies (ACT) threatening to erase the considerable gains against the disease of the  
62 last decade. Alarming, data indicate that for the first time since 2010, progress in  
63 reducing global burden of malaria cases and fatalities nearly flatlined between 2015 and  
64 2017 <sup>1</sup>. New therapies, ideally informed by an understanding of basic parasite biology,  
65 are needed to confront these urgent threats to global malaria control. The study of  
66 malaria-parasite biology and gene-function has traditionally been limited, because  
67 targeted gene-by-gene approaches are laborious and fraught with difficulty due to an  
68 AT-rich (~82%) genome that limits scalability of specific targeted gene-editing methods  
69 (such as CRISPR). Despite the considerable knowledge gene-by-gene studies have  
70 enabled, and the ~two decades that have passed since the *P. falciparum* genome was  
71 completed <sup>2</sup>, the limited throughput of targeted gene-editing strategies combined with  
72 evolutionary distance of *P. falciparum* from classical model eukaryotes has left >90% of  
73 genes untouched experimentally, and ~35% of the parasite's ~5474 genes without  
74 meaningful functional annotation ([www.plasmodb.org](http://www.plasmodb.org)) <sup>3</sup>. High-throughput methods for  
75 functionally profiling the malaria-parasite genome can hasten development of effective  
76 interventions to control a parasite proven to be an adaptable foe.

77

78 Parasite-specific processes essential for parasite survival are naturally attractive as  
79 potential drug-targets, given the decreased likelihood of deleterious off-target effects to  
80 the host. One such process ripe for interrogation is the parasite's survival-response to  
81 the extreme conditions of the host's malarial fever. Repeating fever is a hallmark of all  
82 types of malaria and the cyclical patterns serve as key diagnostic features of infections.  
83 In malignant tertian malaria caused by *P. falciparum*, the 48-hour cycle corresponds to  
84 the parasite's asexual intraerythrocytic-stage life-cycle, wherein parasites invade,  
85 develop, asexually replicate and then rupture their host red blood cell (RBC) to begin the  
86 destructive blood-stage cycle anew. Host fever is triggered by a Type I shock-like  
87 response of the innate immune-system exposure to extracellular parasite debris  
88 released when infected RBCs are lysed during parasite egress. Malarial fever  
89 concomitantly attenuates and synchronizes development of blood-stage *P. falciparum*  
90 infections, as it is lethal to all parasite stages except for early intraerythrocytic ring  
91 stages. However, parasite tolerance of febrile temperatures is crucial for its successful  
92 propagation in human populations as well as a fundamental aspect of malaria  
93 pathogenesis. Previous research suggests parasite-specific factors play a role in  
94 modulating this tolerance for febrile temperatures, though the identities of many of these  
95 factors or the mechanisms by which they operate remain uncertain <sup>4, 5</sup>.

96  
97 We previously used random *piggyBac*-transposon insertional mutagenesis to uncover  
98 genes essential for *P. falciparum* blood-stage survival, generating a saturation-level *P.*  
99 *falciparum* mutant library containing ~38,000 single-disruption mutants <sup>6</sup>. We defined  
100 2680 genes as essential for asexual blood-stage growth, including ~1000 *Plasmodium*-  
101 conserved genes of unknown function. Here we demonstrate the potential of this  
102 *piggyBac*-mutant (*pB*-mutant) library to systematically assign functional annotation to the  
103 *P. falciparum* genome by genome-wide phenotypic screens. In this study, we present the

104 first large-scale forward-genetic functional screen in *P. falciparum* to identify factors  
105 linked to parasite survival of febrile temperatures. Importantly, we functionally annotate  
106 hundreds of parasite genes as critical for the parasite's response to heat shock (HS) but  
107 dispensable under ideal growth-conditions, ~26% of which were previously unannotated  
108 with no known function. Expression-profiling the HS-responses in two different heat  
109 shock-sensitive (HS-Sensitive) *pB*-mutant clones vs. the wildtype parent NF54 via  
110 RNAseq revealed concordance between (1) genes regulated in the parasite's innate  
111 response to HS, (2) the processes dysregulated in these mutants vs. wildtype responses  
112 to HS, and (3) those mutants we identified as HS-Sensitive in our pooled screens.  
113 Together these analyses identify genes and pathways essential in the HS-response,  
114 implicating oxidative stress and protein-damage responses, host-cell remodelling, and  
115 unexpectedly, apicoplast isoprenoid biosynthesis. Apicoplast-targeted genes in general  
116 were up-regulated in response to HS, as were other *Plasmodium* genes with orthologs in  
117 plant and algal genomes. Finally, parallel phenotyping of a mutant library revealed a  
118 significant overlap between parasite pathways underlying the response to febrile  
119 temperatures and those implicated in the artemisinin mechanism of action (MOA),  
120 including oxidative stress, protein-damage responses, and apicoplast-mediated vesicular  
121 trafficking<sup>7,8</sup>. Mutants in known protein-targets of artemisinin tended to be sensitive to  
122 HS<sup>9</sup>, and expression-data from recent field-isolates directly correlates artemisinin-  
123 resistance with HS tolerance in our pooled screen<sup>10</sup>. Further, we found the key K13-  
124 associated parasite endocytosis pathway linked to artemisinin resistance<sup>11,12</sup> is also  
125 downregulated in response to HS. Together these data identify an unexpected link  
126 between artemisinin MOA, HS-survival, and algal origins of the apicoplast, suggesting  
127 the parasite exploits its innate fever-response mechanisms to gain resistance to  
128 artemisinin. This study creates a blueprint for developing a large-scale phenotypic  
129 screening pipeline of the *P. falciparum* *pB*-mutant library to enable high-throughput

130 interrogation of phenotypes of interest to hasten further biological insight that can be  
131 weaponized against the parasite.

132

## 133 **RESULTS**

### 134 **Pooled screens of an extensively characterized pB-mutant clone-library allow** 135 **robust identification of heat-shock phenotypes**

136 To interrogate pathways and processes associated with parasite survival at febrile  
137 temperatures, we developed a large-scale phenotypic screening pipeline to analyze the  
138 phenotypes in pooled *pB*-mutant parasites exposed to HS-induced stress (Fig. S1). We  
139 previously demonstrated using individual clonal *pB*-mutant parasite lines that mutant  
140 growth-phenotypes can be detected and differentiated in pooled screening utilizing  
141 QIseq—"Sensitive" mutants with disruptions in genes/genomic features important for  
142 growth have lower QIseq reads, while "Neutral" disruptions in features not vital for  
143 growth under the same conditions have higher reads<sup>13</sup>. We therefore reasoned that  
144 mutants with mutations in genes underlying the HS-response would grow poorly in  
145 response to HS compared to mutants in genes not contributing to HS-survival.

146

147 We used a pool of 128 unique, extensively characterized *P. falciparum* *pB*-mutant clones  
148 reflecting disruptions in genes spanning a range of functional categories, as well as  
149 many genes without existing functional information, as a "pilot-library" for initial  
150 phenotypic screen-development (<sup>13, 14</sup>; Methods, *Generating the pilot-library of pB-*  
151 *mutant parasite clones*). An *in vitro* HS-screen of this pilot-library, adapted from a  
152 phenotype-screen of many *pB*-mutant-clones comprising the pilot-library<sup>15</sup>, defined *pB*-  
153 mutant HS-response phenotypes to fever-like temperatures (Fig. 1A-E, Table S1A-C,  
154 Methods). We next calculated a measure of fitness for each mutant in response to HS  
155 while also taking into account inherent differences in mutant-growth in ideal conditions,

156 which we termed the Phenotypic-Fitness Score in response to HS (PFS<sub>HS</sub>; Methods).  
157 The PFS<sub>HS</sub> result was consistent with a previously reported flow cytometry-based assay  
158 of 25 individual *piggyBac*-mutant clones in response to heat-shock (Wilcoxon  $p < 0.01$ ,  
159 Fig 1F; <sup>15</sup>). We classified 28 mutants of the pilot-library as HS-Sensitive (Fig. 1E-H,  
160 indicated in red; Table S1A-C). Fourteen mutants performed poorly in both the Growth-  
161 and HS-Screens (Fig. 1E,G, yellow). We classified 28 mutants displaying a slight growth  
162 advantage in response to HS (Fig. 1E,G, green) as “HS-Tolerant”. Mutants exhibiting  
163 neither sensitivity nor tolerance to HS were classified as HS-Neutral ( $n = 49$ ).

164

165 Qlseq-data resulting from the HS- and Growth-screens allowed robust assignment of  
166 mutant-phenotypes for both (see Methods). We primarily classified mutants sensitive to  
167 heat-shock alone as HS-Sensitive to avoid possible over-interpretation of generally-sick  
168 Growth-Sensitive mutants (Fig. 1G-H).

169

170 **Pooled phenotypic screens scaled up to a 1K *pB*-mutant library enable**  
171 **identification of processes driving the *P. falciparum* heat-shock response**

172 We next scaled our pooled HS-screen to a mutant library of 922 functionally  
173 uncharacterized mutants using the methods we established in our pilot-library screens  
174 (Table S2A-C). This 1K-library comprised 12 large mixed-population pools of uncloned  
175 mutants randomly selected from our saturation library and subjected to phenotypic  
176 screens in parallel. Insertion-sites were unknown until the 1K-library HS-Screen and  
177 Qlseq were completed. Mutants were ranked by fold-change growth in response to HS  
178 from HS-Sensitive to HS-Tolerant, as per cut-offs determined from our pilot-library  
179 screens. Our analysis distinguished 149 mutants growing well in ideal growth conditions  
180 but poorly in response to HS as HS-Sensitive (Fig. 2A), while 91 mutants performed  
181 poorly in both the Growth- and HS-screens. Of the remaining mutants, 139 HS-Tolerant

182 mutants had slightly better growth in HS than ideal growth-conditions, while 543  
183 classified as HS-Neutral were neither sensitive nor tolerant.

184

185 This larger scale of screening covering genes annotated to diverse GO-categories, as  
186 well as many genes of unknown function, allowed us to assess gene functional-  
187 enrichment in HS-Sensitive and Growth-Sensitive phenotypic categories vs all other  
188 mutants in the 1K-library. HS-Sensitive mutants were enriched in GO terms associated  
189 with HS-response such as protein-folding, response to DNA-damage, DNA-repair, and  
190 regulation of vesicle-mediated transport, broadly in agreement with processes identified  
191 to underlie the HS-response by more conventional gene expression-based methods <sup>4, 5</sup>.  
192 Growth-Sensitive mutants tended to be enriched for more general categories broadly  
193 important for survival in all conditions, such as translation- or mRNA-metabolism-related  
194 terms (Fig. 2B), as might be expected given the high essentiality of these processes in  
195 ideal growth <sup>6, 16</sup>.

196

197 **Increased transcription of the unfolded protein response (UPR), organelle-**  
198 **targeted stress-response pathways and host-cell remodeling characterize the**  
199 **parasite HS-response**

200 We first characterized the wildtype parent-NF54 transcriptome in response to HS to  
201 establish a baseline for comparison using an experimental design similar to a prior study  
202 assessing transcriptional changes in response to febrile temperatures via microarray <sup>5</sup>.  
203 The HS assay-design mimicking parasite exposure to malarial fever was modelled after  
204 conditions we established for our pooled-screens (Methods). RNAseq was performed on  
205 heat-shocked parasites vs. a non-heat-shocked control. Genes identified as differentially  
206 expressed in response to febrile temperatures vs. 37°C were classified into three  
207 different categories based on direction of response in the wildtype parasite: (1)



208 upregulated in response to HS; (2) downregulated in HS, and (3) neutral in HS (Fig. 3A-  
209 B, Table S3A-D). The majority of genes expressed above threshold in our analysis were  
210 HS-neutral (1541 genes out of 2567, or ~60%) and were enriched for genes involved in  
211 general housekeeping functions such as the proteasome core complex (ubiquitin-  
212 proteasome system), the ubiquitin-dependent ERAD-pathway, and regulators thereof),  
213 RNA metabolism (RNA-binding, mRNA-splicing) and transport functions (e.g. protein  
214 import into nucleus, vesicle-mediated transport). We primarily considered genes  
215 upregulated in HS as drivers of the HS-response.

216

217 Genes upregulated in HS ( $\uparrow$ ,  $n = 415$ ) tended to be enriched for processes such as  
218 protein-folding, unfolded protein-binding, response to heat, mitochondrial processes, and  
219 host-cell remodelling-associated exported proteins localizing to the Maurer's clefts (Fig.  
220 3B, Table S3C-D). Genes downregulated in HS ( $\downarrow$ ,  $n = 611$ ) tended to be enriched for  
221 pathogenesis-related functions and components of the parasite invasion machinery,  
222 such as entry/exit from the host cell and cell-cell adhesion, and organelles including the  
223 inner-membrane pellicle complex, micronemes, and rhoptries. These data are in general  
224 agreement with previously-reported processes expected to drive the parasite HS-  
225 response <sup>4, 5</sup>.

226

227 We reasoned that genes dysregulated in HS-Sensitive mutants compared to wildtype  
228 underlie the HS-response. We chose two individual HS-Sensitive mutant clonal lines  
229 satisfying several careful criteria for additional profiling via RNAseq to identify  
230 dysregulated genes responsible for this sensitivity:  $\Delta DHC$  and  $\Delta LRR5$  (dynein heavy-  
231 chain gene PF3D7\_1122900 and leucine-rich repeat protein PF3D7\_1432400). Criteria  
232 for selection: i) Specificity of phenotype. Both mutants are highly sensitive to heat shock  
233 (PFS < 0.1), but under ideal culture conditions grow better than most other mutants in

234 the pilot library (exhibiting higher fold change than 95.3% and 83.6% mutants,  
235 respectively). ii) Clear functional consequences of disruption. Both are presumed loss-of-  
236 function mutants with a single disruption in the coding region of a gene determined to be  
237 dispensable for asexual blood-stage growth under ideal culture conditions<sup>6</sup>. iii) GO  
238 classification. GO classifications of LRR5 and DHC are representative of the broad  
239 functional categories we found to be associated with heat response in our earlier small  
240 screen<sup>15</sup> and other reports (regulating gene expression and intracellular vesicular  
241 transport, respectively), yet interactions between these pathways are undefined. Finally,  
242 iv) Clonal phenotype validation. Both mutant lines were validated in a heat shock assay  
243 of individual clones<sup>15</sup>, but otherwise these genes were not previously implicated in the  
244 HS-response of malaria parasites.

245

246 The 1298 genes which could be classified into HS-response categories across all three  
247 parasites were analyzed for functional-enrichment (Table S3B). The majority of genes  
248 were HS-neutral across all three parasites and were enriched for essential  
249 housekeeping functions (n = 615; Table S3B-D). We reasoned these non-HS-regulated  
250 genes have functions too important for basic survival to tolerate large stress-associated  
251 expression-changes, and these genes were not considered drivers of the HS-response.  
252 We identified 94 genes significantly upregulated in HS across all three parasites (↑↑↑),  
253 which were functionally enriched for protein-folding, chaperone-related processes, and  
254 other processes related to heat-stress and the UPR, in agreement with previous  
255 expression-based studies<sup>5</sup>, as well as enrichment-results from HS-Sensitive mutants in  
256 our pooled screening, indicating the parasite increases production of heat-shock proteins  
257 (HSPs) and associated chaperones to repair the glut of proteins damaged/misfolded by  
258 heat-stress (Table S3B-D). Energy-producing processes (gluconeogenesis, glycolysis)  
259 were also upregulated, suggesting the parasite reroutes anabolic metabolism to increase

260 energy production to support ATP-dependent processes such as protein-refolding to  
261 correct heat-damaged proteins. Genes upregulated in HS were further enriched for  
262 processes involved in host-cell remodeling, including genes targeted to the Maurer's  
263 clefts, the host cell, and intracellular vesicles—all known to be important for parasite-  
264 remodeling of the host-cell to promote structural reinforcement against heat-shock  
265 damage to ensure its own survival<sup>4,5</sup>. Organellar targeting to the mitochondria and  
266 apicoplast are also enriched in upregulated HS-responsive genes. The parasite's  
267 increased utilization of mitochondrial stress-response pathways may aid in degrading  
268 heat-damaged proteins that cannot be correctly refolded. Increased activity in the food  
269 digestive vacuole may allow the parasite to phagocytose and eliminate toxic misfolded  
270 protein-aggregates. The apicoplast involvement, particularly the isoprenoid biosynthesis  
271 pathway, has not been previously implicated in the HS-response.

272

273 Genes downregulated in all three parasites in response to HS (↓↓↓, n = 205) were  
274 enriched for virulence-factor and invasion-machinery-associated GO terms, suggesting  
275 the parasite decreases production of transcripts associated with pathogenesis, invasion  
276 and egress, lengthening its intracellular recovery-time to address global protein-damage.

277

278 Both HS-Sensitive mutants share many characteristic features of the wildtype response  
279 to febrile temperatures, which likely enabled their survival (Fig. 3A-B, red, blue; Table  
280 S3C-D). We identified two primary expression categories of genes dysregulated in the  
281 HS-Sensitive mutants: (1) genes upregulated in the wildtype HS-response that were  
282 otherwise dysregulated in the HS-Sensitive mutants, which we interpreted as loss-of-  
283 function changes (↑↘↘, n=83), and (2) genes that were not regulated in response to HS  
284 in the wildtype but were upregulated in the HS-Sensitive mutants (– ↑↑, n = 74),

285 presumably equivalent to dominant-negative gain-of-function changes (Fig. 3A-B, ochre  
286 and tan, respectively). This first category of mutant-dysregulated genes ( $\uparrow^{\times\times}$ ) was  
287 enriched for the UPR, as well as mitochondrial and apicoplast-localized pathways  
288 (cytochrome oxidase-assembly and fatty-acid biosynthesis, respectively). Several  
289 apicoplast isoprenoid biosynthesis-related genes upregulated in the wildtype HS-  
290 response were additionally dysregulated in one or both HS-Sensitive *pB*-mutant clones  
291 (Fig. 3C). The second category of mutant-dysregulated genes ( $-\uparrow$ ), those that are not  
292 HS-responsive in wildtype, were enriched for translation-associated processes.

293

294 These data taken together suggest underlying mechanisms responsible for the HS-  
295 response. Critically, HS-Sensitive mutants fail to upregulate mitochondrial and apicoplast  
296 stress-response pathways, as well as signal peptide-processing pathways that might  
297 enable appropriate activation of those pathways. Mutants do not increase production of  
298 transcripts associated with responding to unfolded proteins. HS-Sensitive mutants  
299 additionally upregulate translation-related processes in response to HS when translation  
300 should be paused or neutral. This increase may overwhelm the parasite's capacity to  
301 repair or degrade heat-damaged proteins, exacerbating the formation/accumulation of  
302 toxic misfolded-protein aggregates that increase parasite sensitivity to HS.

303

### 304 **Apicoplast isoprenoid biosynthesis is critical for *P. falciparum* survival of febrile** 305 **temperatures**

306 We examined our RNAseq data more closely to discern contributions of the apicoplast to  
307 HS-survival (Fig. 4A-E; Table S4A-D). We found that apicoplast-targeted genes tended  
308 to be increased in response to HS as compared to all non-apicoplast-targeted genes  
309 (Fig. 4A), were more likely to be essential during ideal blood-stage growth conditions

310 (Fig. 4B), were enriched for stress-response processes such as the UPR and oxidative-  
311 stress, and less expectedly, isoprenoid biosynthesis (Fig. 4C). As a major function of  
312 isoprenoid biosynthesis is in protein-prenylation—an important post-translational  
313 modification that regulates protein-targeting and function throughout the cell—we  
314 hypothesized that mutants in known-prenylated proteins<sup>17, 18</sup> would also have a  
315 phenotype in HS. We examined our 1K mutant-library for representation of isoprenoid  
316 biosynthesis, its immediate upstream-regulators (proteins responsible for modulation  
317 and import of glycolytic intermediates that serve as pathway substrates), and immediate  
318 downstream-effector proteins, and found that all eight isoprenoid biosynthesis-related  
319 *pB*-mutants included in the pooled screen were indeed HS-Sensitive (Fig. 4D, Table  
320 S4C).

321

322 Based on these data we further hypothesized that proteins or pathways allowing *P.*  
323 *falciparum* survival of febrile temperatures would be absent or otherwise divergent in  
324 *Plasmodium* species whose hosts do not mount fever-responses. We therefore  
325 compared the apicoplast isoprenoid biosynthesis pathway between *P. falciparum* and  
326 two rodent-infective species, *P. berghei* and *P. yoelii*. We found key thiamine-synthesis  
327 enzymes directly upstream of the pathway missing in the rodent-infective malaria  
328 parasites, including hydroxy-ethylthiazole kinase (ThzK); ThzK is up-regulated in the  
329 canonical parasite response to febrile temperatures and dysregulated in HS-Sensitive  
330 mutants (Fig. 4E, Table S4C-D). Perhaps most importantly, DOXP-Synthase (DXS), the  
331 critical enzyme marking the first step in isoprenoid biosynthesis, is upregulated in HS,  
332 dysregulated in HS-Sensitive mutants, and was HS-Sensitive in pooled screening, as  
333 were all four members of the prenylated blood-stage proteome represented in our  
334 screen (Fig. 4E, Table S4C-D). These data taken together strongly implicate isoprenoid  
335 biosynthesis in the HS-response.

336

337 Though the apicoplast has not previously been implicated in parasite survival of febrile  
338 temperatures, there is extensive literature on the ability of plants to mount effective  
339 defenses against heat as well as other external stressors, particularly critical for non-  
340 motile organisms at the mercy of their environments. We investigated the relationship  
341 between the parasite's HS-response and "plant-like" stress-responses by evaluating  
342 phyletic distribution of parasite HS-response genes in representative plant and algal  
343 genomes. *P. falciparum* genes with plant orthologs indicating potential endosymbiont-  
344 ancestry tended to be increased in response to HS vs. genes that do not have plant  
345 orthologs (Fig. 4F). These lines of evidence considered together present an evolutionary  
346 explanation that endosymbiosis of the apicoplast's algal progenitor enabled parasite-  
347 survival of extreme temperatures.

348

#### 349 **Processes enabling parasites to survive fever also drive resistance to artemisinin**

350 We noted similarities between processes we identified to be driving the parasite HS-  
351 response and those implicated in parasite-resistance to artemisinin<sup>7, 8, 10</sup>. Therefore, we  
352 did a series of parallel phenotype-screens of our *pB*-mutant pilot-library using sublethal  
353 concentrations of two artemisinin compounds (dihydroartemisinin, DHA; artesunate, AS),  
354 heightened conditions of oxidative stress of RBCs, and exposure to a proteasome  
355 inhibitor (Bortezomib; BTZ) to investigate the possible relationship between HS-  
356 response and artemisinin MOA, as well as Oxidative-Screens (Fig. 5A, Table S5, Fig.  
357 S2A, Methods) . We found that HS-Sensitive mutants tended to be sensitive to both  
358 artemisinin derivatives and H<sub>2</sub>O<sub>2</sub>-induced oxidative stress, while HS-Tolerant mutants  
359 were less sensitive to either condition (Fig. 5A). Also, HS-Sensitive mutants shared an  
360 increased sensitivity to the proteasome inhibitor BTZ, consistent with laboratory  
361 observations connecting artemisinin MOA to the proteasome and clinical data that

362 proteasome-inhibitors act synergistically with artemisinins<sup>8, 19, 20, 21</sup>. Overall, correlation  
363 of mutant phenotypic profiles across screens varied, with 16-45% having correlating  
364 phenotypes in at least one additional screen (Fig. 5B, Fig. S2B).

365

366 We next assessed whether these laboratory-based experimental findings corresponded  
367 to 'real world' changes associated with *P. falciparum* in artemisinin-resistant (ART-R)  
368 clinical isolates<sup>10</sup>. Consistent with our laboratory findings linking HS-sensitivity and  
369 ART-sensitivity, we found that genes mRNA levels of HS-Sensitive genes are  
370 significantly positively correlated with parasite clearance half-life under treatment with  
371 artemisinin-based combination therapies in recent field-isolates compared with HS-  
372 Tolerant genes<sup>10</sup> (Fig. 5C, Tables S2 and S6). We also compared genes by HS-  
373 response expression category to mRNA expression levels in these field isolates, finding  
374 that genes upregulated in response to heat stress are significantly positively correlated  
375 with parasite clearance half-life, while genes downregulated in response to heat stress  
376 are more likely to be negatively correlated (Fig 5D, Tables S3 and S6). Therefore, we  
377 conclude the parasite's responses to heat shock mirror the responses to artemisinin as  
378 both are similar types of cellular stress on the parasite. Both of these stressors induce  
379 unfolded protein responses, which include both upregulation and down regulation of  
380 metabolic activities that enable the parasite to tolerate the toxic effects of accumulating  
381 damaged proteins. The upregulated processes include the proteasome core and  
382 chaperones to degrade or refold damaged proteins, while many other aspects of  
383 metabolism, including growth-related anabolic processes, are down regulated to prevent  
384 build-up of new proteins that may be damaged.

385

386 Artemisinin is activated by degradation of host hemoglobin. Recent evidence has  
387 suggested two key, temporally-distinct ART-R mechanisms: (1) a multi-functional protein

388 long associated with resistance in field-isolates, *kelch13* (K13) confers resistance  
389 upstream of hemoglobin degradation by modulating an associated endocytosis pathway;  
390 and (2) downstream of hemoglobin degradation through the ubiquitin-proteasome  
391 system (UPS), where K13 may function as or regulate a ubiquitin ligase<sup>10, 11, 12, 22, 23, 24, 25</sup>.  
392 In upstream-resistance, endocytotic transport of hemoglobin to the digestive vacuole  
393 (DV) is down-regulated as this is the key process through which the parasite ingests,  
394 degrades, and then releases hemoglobin. K13 mutant-isolates appear to downregulate  
395 processes along this endocytosis pathway, decreasing parasite hemoglobin digestion  
396 and release of heme to activate artemisinin, thereby increasing parasite survival. We  
397 found that K13-defined endocytosis is also downregulated in response to HS (Fig. 5E).  
398 As the K13-mediated endocytosis pathway culminates in host haemoglobin-cargo being  
399 degraded in the DV, we further assessed our 1k HS-screen for DV-associated proteins.  
400 We found DV-associated proteins did tend to be sensitive to heat-shock, including key  
401 DV resident-proteases (Plasmepsin I, M1-family alanyl aminopeptidase; Fig. S3A)<sup>26</sup>. We  
402 next evaluated our 1K-library HS-Screen for direct K13-interacting partner-proteins  
403 recently identified via immunoprecipitation<sup>25</sup>, and found that mutants in 10 of the 24  
404 unique putative K13-partner-proteins represented in the screen were sensitive to HS.  
405 Further, 5 of 7 known alkylation-targets of artemisinin represented in our screen had  
406 sensitivity to HS<sup>9, 26</sup> (Fig. S3B). We noted significant overlap in each of these categories  
407 of ART MOA-related genes and isoprenoid biosynthesis-related genes (Fig. S3C).  
408  
409 In a second downstream step post-activation of artemisinin, the parasite engages the  
410 UPS to further mitigate artemisinin-induced damage. Artemisinins mount a multi-pronged  
411 attack against the parasite by causing a global, non-specific accumulation of damaged  
412 parasite proteins, which are then polyubiquitinated/marked for degradation, while also  
413 inhibiting proteasome-function. These poly-ubiquitinated proteins ultimately overwhelm



414 the parasite's decreased capacity for UPS-mediated protein-degradation<sup>8</sup>. Key  
415 ubiquitinating components of this system, including E2/E3 ligases and K13, are  
416 downregulated in response to HS, while key components of the UPR and protein folding  
417 are increased (Fig. 5E). In contrast, components of the core proteasome were  
418 universally increased in response to HS when considered in aggregate, although the  
419 change did not meet our fold-change criteria for being HS-regulated (Fig. S4A).  
420  
421 Synthesizing these data, we present a model for the relationship between what is  
422 currently understood of artemisinin MOA and HS-response (Fig. 5F). The canonical  
423 parasite-response to fever is to increase protein-folding and UPR while inhibiting  
424 ubiquitination to prevent accumulation of toxic, polyubiquitinated protein-aggregates. The  
425 parasite simultaneously increases its capacity for proteasome-mediated degradation—  
426 ultimately enabling it to resolve HS-instigated stress and thus survive febrile  
427 temperatures (Fig. S4B). As heat-stress is also injurious to the host RBC, the parasite  
428 diverts resources to stabilize the host cell—increasing export and trafficking of proteins  
429 involved in host-cell remodeling that support fortification of the host-cell membrane, as  
430 well as decreasing uptake of host-cell hemoglobin through the K13-mediated  
431 endocytosis pathway—processes which are ultimately driven by prenylation downstream  
432 of apicoplast isoprenoid biosynthesis. Artemisinins kill by overwhelming these same  
433 pathways: damaging and unfolding proteins, preventing folding of newly synthesized  
434 proteins and inhibiting the proteasome, while at the same time activating ubiquitination-  
435 machinery to ensure the accumulation of toxic polyubiquitinated proteins that eventually  
436 cause cell-death. ART-R-associated mutations allow the parasite to constitutively  
437 activate unfolded-protein response mechanisms which increase its capacity for refolding  
438 or degrading those toxic proteins<sup>27</sup>. The overall increase in damaged-protein  
439 degradation-capacity allows ART-R parasites to keep up with the influx of artemisinin-

440 induced protein-damage, clearing the waste and enabling parasite survival. This direct  
441 inverse relationship in activation of endocytosis, the ubiquitin-proteasome system and  
442 other pathways underlying DHA-mediated killing and febrile-temperature survival,  
443 supports a shared mechanism for artemisinin-resistance and HS-response, suggesting  
444 that ART-R parasites evolved to harness canonical HS-survival mechanisms to survive  
445 artemisinin.

446

#### 447 **Discussion**

448 Our data indicate that the parasite crisis-response to HS is multi-faceted to relieve the  
449 build-up of heat-damaged proteins before it is overwhelmed by toxic, misfolded-protein  
450 aggregates. Responding to or perhaps preventing a build-up of potentially toxic heat-  
451 damaged proteins, the parasite upregulates expression of chaperones to stabilize and  
452 detoxify them, downregulating ubiquitinating enzymes to discourage their aggregation  
453 while upregulating the core proteasome and vesicular trafficking to degrade and  
454 eliminate proteins which can't be repaired. Equally important in the survival-response are  
455 changes in redox homeostasis, lipid metabolism, cellular transport, and metabolic  
456 processes associated with the endosymbiont-derived organelles. The parasite requires  
457 increased energy to mount this febrile response, which it provides by redirecting its own  
458 internal biosynthetic pathways to produce glucose. Interestingly, we confirm the  
459 parasite's protective response-mechanisms include proteins exported into the  
460 erythrocyte, suggesting that the parasite's metabolic processes exported to remodelled  
461 cytoplasm of the parasitized host cell are equally vulnerable and vital to malaria parasite  
462 survival.

463

464 The apicoplast genes have a higher proportion of up-regulated genes in HS and tend to  
465 be essential under normal growth situation. (Fig. 4A,B). The apicoplast isoprenoid

466 biosynthesis pathway's critical involvement in survival of febrile temperatures is  
467 nevertheless a surprise, as it has not been implicated before in the *Plasmodium* HS-  
468 response. Isoprenoids are required for myriad functions across the tree of life—plant  
469 chloroplasts, algae, some parasitic protozoa and bacterial pathogens utilize a  
470 specialized form of this pathway absent from all metazoans (also called the MEP or  
471 DOXP non-mevalonate pathway), which has made isoprenoid biosynthesis an attractive  
472 target for intervention against a range of pathogens<sup>28, 29</sup>. Most studied organisms make  
473 wide use of protein-prenylation and have large prenylated proteomes; malaria parasites,  
474 in contrast, have a very small prenylated blood-stage proteome (~20 proteins) consisting  
475 primarily of vesicular trafficking proteins, notably the Rab-family GTPases<sup>17, 18</sup>. Recent  
476 studies indicate the key essential function of isoprenoids in the parasite blood-stage is in  
477 their roles as substrate for protein-prenylation—specifically, in prenylating proteins  
478 driving vesicular transport to the digestive vacuole<sup>30, 31</sup>. In the absence of prenylation,  
479 Rab5 trafficking is disrupted, which leads to digestive vacuole-destabilization and  
480 parasite death<sup>31</sup>. Notably, artemisinin also disrupts digestive vacuole-morphology,  
481 resulting in a very similar phenotype as a consequence of its activation via hemoglobin  
482 digestion<sup>32, 33</sup>. Intriguingly, recent data confirm the association of key resistance-  
483 mediator K13 with Rab-GTPases<sup>25</sup>, adding to the repertoire of proteins comprising K13-  
484 mediated endocytic vesicles, and by extension supporting the role of prenylation in K13-  
485 mediated processes associated with ART MOA.

486

487 Another key parasite-defense against oxidative stress induced by pro-oxidant  
488 compounds (such as artemisinin) includes increased vitamin E biosynthesis—another  
489 exclusive function of the MEP isoprenoid-biosynthesis pathway, whose stress-related  
490 regulation has been extensively studied in plants<sup>34, 35</sup>. Further insights to the role  
491 isoprenoids play in the HS-response may be gleaned from plants and pathogenic

492 bacteria, where research suggests key branchpoint-enzyme DXS, which catalyzes the  
493 first and rate-determining step of the MEP pathway<sup>36</sup> has a role in sensing and then  
494 facilitating adaptation to ever-changing environmental conditions, including temperature,  
495 light-exposure, chemical compounds, and oxidative stress (for example<sup>37, 38</sup>). Elevated  
496 levels of isoprenoids have been found to correlate with plant exposure to drought and  
497 other stressors and are considered a key component of plant-defenses against abiotic  
498 stress<sup>39</sup>. The DXS ortholog may play a similar role in *P. falciparum*, enabling the  
499 parasite to mount quick responses to unfavorable conditions in the host-environment,  
500 such as fever.

501

502 Interestingly, concurrent studies now provide mechanistic insights illuminating the  
503 biochemical relationship between apicoplast isoprenoid biosynthesis and the parasite  
504 febrile-temperature survival response<sup>40</sup>. Farnesylation of HSP40 (PF3D7\_1437900), a  
505 type of prenylation mediated by the MEP pathway, is critical for *P. falciparum* survival of  
506 thermal stress. In this study inhibition of isoprenoid biosynthesis ultimately resulted in  
507 reduced association of HSP40 with critical components of the cytoskeleton, protein-  
508 export, and vesicular transport pathways—without which *P. falciparum* could survive  
509 neither heat nor cold stress. Suppression of these cellular processes by loss of HSP40-  
510 farnesylation directly corresponds to HS-sensitive pathways identified via both our  
511 forward-genetic screen and our gene-expression analyses of the HS-Sensitive LRR5-  
512 and DHC4-mutant clones.

513

514 Few eukaryotes are known to be able to thrive in extreme-heat environments; most are  
515 unable to complete their lifecycles above 40°C<sup>41</sup>. The survival mechanism of malaria  
516 parasites could be attributed to the algal ancestral lineage of the apicoplast. Some  
517 extant red algal-lineages (genus *Cyanidioschyzon*) are extremophilic inhabitants of

518 acidic hot-springs and are remarkably resistant to heat shock up to 63°C; green-algae  
519 *Chlamydomonas reinhardtii* was also able to survive to 42°C<sup>42</sup>. Responsibility for this  
520 extreme resistance to transient exposure to high temperatures was attributed to two  
521 genes of the small heat shock protein (sHSP) family (CMJ100C and CMJ101C). The *P.*  
522 *falciparum* ortholog for these genes (PF3D7\_1304500) was upregulated in the wildtype  
523 HS-response and dysregulated in both our HS-Sensitive mutants, indicating its  
524 contribution to parasite survival in extreme temperatures. Mutations in this gene were  
525 not represented in our pooled screens.

526

527 It is tempting to speculate that presence of the endosymbiont cyanobacterium-related  
528 ancestral genes and its associated plant stress-response mechanisms is what enabled  
529 the ancestral parasite to survive host-fever, likely an important and early step leading to  
530 successful infection of hominid hosts. Our findings of significant overlap between  
531 parasite-responses to three disparate stressors (HS, artemisinin, oxidative stress) offers  
532 new insight into how *P. falciparum* exhibited artemisinin-resistance even in the initial  
533 clinical trials<sup>43</sup>, and then further evolved resistance relatively quickly after mass-  
534 introduction of the drug by “hijacking” and repurposing the parasite’s in-built fever-  
535 response pathways.

536

### 537 **Conclusion**

538 Deeper knowledge of parasite biology is expected to enable more effective and likely  
539 longer-lasting antimalarial interventions. Similarly, a better mechanistic understanding of  
540 artemisinin MOA will lead to better combination therapies to combat emerging  
541 resistance. With this first large-scale forward-genetic screen in *P. falciparum*, we  
542 revealed the parasite’s survival responses to malarial fever and artemisinin

543 chemotherapy share common underpinnings that heavily depend on metabolic  
544 processes of plant origin.  
545  
546 ART-R ultimately hinges on highly efficient protein-degradation mechanisms. This  
547 mechanistic knowledge allows for the application of intelligently considered counters to  
548 ART-R, such as combinatorial therapy with proteasome-inhibitors, which has  
549 experimentally shown great promise <sup>44</sup>. Our current study highlights the potential of  
550 forward-genetic screens to elucidate unexpected processes and pathways, such as  
551 DOXP and isoprenoid biosynthesis, that are associated with the artemisinin MOA which  
552 may serve as synergistic druggable targets <sup>45</sup>. Future studies can exploit a genome-wide  
553 screening approach to iteratively ascribe function to every part of the malaria-parasite  
554 genome to support targeted development of new, more-efficacious antimalarial  
555 combination therapies to limit and potentially reverse artemisinin resistance.

556

#### 557 **Declarations**

558 *Ethics approval and consent to participate*

559 Not applicable.

560

561 *Consent for publication*

562 Not applicable.

563 *Availability of data and materials*

564 The raw RNAseq dataset supporting the conclusions of this article are available in the  
565 Mendeley Data repository *Malaria-parasite survival of host fever is linked to artemisinin*  
566 *resistance*, <http://dx.doi.org/10.17632/b8g3wbnd5v.1> <sup>46</sup>. Raw QIseq dataset accession  
567 numbers are listed in Table S5.

568

569 *Competing interests*

570 The authors declare that they have no competing interests.

571

572 *Funding*

573 This work was supported by the National Institutes of Health grant R01 AI094973 and

574 R01 AI117017 (J.H.A.) and the Wellcome Trust grant 098051 (J.C.R.).

575

576 *Authors' contributions*

577 Conceptualization, M.Z., C.W., J.O., T.D.O., J.C.R., M.T.F., R.H.Y.J., and J.H.A.;

578 Methodology, M.Z., C.W., J.O., K.B.S., R.H.Y.J., and J.H.A.; Software, J.O. and C.W.;

579 Validation, M.Z., C.W., and J.O.; Formal Analysis, M.Z., C.W., J.O., S.R.A., and

580 R.H.Y.J.; Investigation, M.Z., C.W., J.O., P.T., D.C., S.B., S.X., M.M., and R.H.Y.J.; Data

581 Curation, M.Z., C.W., and J.O.; Writing—Original Draft, J.O., M.Z., and J.H.A.; Writing—

582 Review & Editing, J.O., M.Z., T.D.O., J.C.R. and J.H.A.; Visualization, C.W., M.Z., J.O.,

583 and R.H.Y.J.; Supervision, M.Z., J.O., T.D.O., J.C.R., M.T.F., R.H.Y.J., and J.H.A.;

584 Project Administration, M.Z.; Funding Acquisition, J.C.R. and J.H.A.

585

586 *Acknowledgements*

587 We appreciate the Wellcome Sanger Institute (United Kingdom) for performing Qlseq

588 and Xiangyun Liao, Suzanne Li, and Kenneth Udenze for support of parasite cell culture.

589 We thank the USF Genomics Program Omics Hub for productive discussion.

590

591 **FIGURE LEGENDS**

592 **Figure 1. Pooled screens of *P. falciparum* piggyBac mutants allow robust**

593 **identification of heat-shock phenotypes. A.** Experimental design for pooled heat

594 shock (HS) phenotypic screens. The pilot-library of *pB*-mutant clones (n=128) was  
595 exposed to three rounds of temperature-cycling (41°C for 8 hours) to simulate malarial  
596 fever (Methods, Pooled-screen assay-design). A pilot-library control concurrently grown  
597 continuously at 37°C established inherent growth of each *pB* mutant. HS screens of the  
598 pilot-library were conducted in biological duplicate and technical triplicate and were  
599 highly correlated, indicating high accuracy and reproducibility (See Fig. S5A; Methods,  
600 Pooled-screen assay-design, HS-Screen).

601 **B.** Qlseq quantifies each *pB*-mutant in the pilot-library from sequence-reads of the 5' and  
602 3' ends of each *pB* insertion-site. Colored lines represent genes. Black boxes indicate  
603 transposon location (Fig. S5B; Methods, Qlseq).

604 **C.** Pilot-library mutant growth-phenotypes at ideal temperatures, defined as fold change  
605 in Qlseq reads-count after three cycles growth at 37°C (FC-Growth; Methods) ranked  
606 from Sensitive to Tolerant. Mutants with inherently slower or faster growth under ideal  
607 conditions are shown in grey and blue, respectively.

608 **D.** Pilot-library mutant HS-phenotypes ordered from Sensitive (red) to Tolerant (green).  
609 Mutant growth was defined as Qlseq reads-count fold-change in response to HS (FC-  
610 HS) vs. non heat-shocked control (Methods). HS-Sensitive mutants have lower FC-HS  
611 (red, FC-HS < 1), while HS-Tolerant mutants have higher FC-HS (green, FC-HS > 1).

612 **E.** HS- and Growth-phenotypes of the pilot-library mutants. HS-phenotype of each  
613 mutant (displayed as line-graph) is superimposed on its corresponding Growth-  
614 phenotype (bar graph). \*Known HS-Sensitive and \*\*HS-Tolerant *pB*-mutant clones  
615 served as benchmarks in the pilot-library HS-Screen for identifying sensitive/tolerant  
616 mutants<sup>15</sup>.

617 **F.** Phenotype-comparison between mutants characterized in both individual HS-assays<sup>15</sup>  
618 and pooled HS-screening (n = 20). Mutant clones without an observed phenotype in  
619 individual HS-assay as determined by above-average growth via flow cytometry (green)



620 also had significantly higher Phenotypic Fitness Scores in response to HS ( $PFS_{HS}$ ) in  
621 pooled screening, while mutant clones characterized as HS-Sensitive in individual  
622 assays (red) also had significantly lower  $PFS_{HS}$  in pooled screening. (\*\* p-value < 0.01,  
623 Mann-Whitney U test),  
624 **G.** Mutant heat-shock phenotype classifications. Red = HS-Sensitive mutants ( $FC_{HS} <$   
625  $0.5$  and  $PFS_{HS} < 0.25$ ,  $n = 28$ ). Yellow = mutants classified as both Growth-Sensitive and  
626 HS-Sensitive ( $FC_{HS} < 0.5$ ,  $PFS_{HS} > 0.25$ ,  $n = 14$ ). Green = HS-Tolerant mutants ( $FC_{HS} >$   
627  $1.5$ ,  $n = 30$ ). Mutants neither Sensitive nor Tolerant to HS were classified as HS-  
628 Neutral ( $n = 49$ ) (Methods) .  
629 **H.** Distributions of  $PFS_{HS}$  for mutant HS-phenotype classifications. HS-Sensitive mutants  
630 are assigned the lowest  $PFS_{HS}$ , while HS-Tolerant mutations are assigned the highest  
631  $PFS_{HS}$  (\*\*\*\* Wilcoxon-test p-value <  $1e-15$ ).

632

633 **Figure 2. Large-scale pooled phenotypic screens enable identification of**  
634 **processes driving the *P. falciparum* heat-shock response.**

635 **A.** HS-Sensitive mutations identified in pooled screens of 1K-library of 922 *pB*-mutants  
636 (Table S2). The uncloned, large mixed-population pools comprising the 1K-library ( $n =$   
637  $10$ ) were parallelly screened in both ideal growth conditions and under HS, and mutants  
638 were assigned phenotypes as per methods established in the pilot-library screens (Fig.  
639 1, Table S1, Methods). Mutants are ranked by fold-change in response to HS from HS-  
640 Sensitive (red;  $n = 149$ ,  $FC_{HS} < 0.5$  and  $PFS_{HS} < 0.25$ ) to HS-Tolerant (green;  $n = 139$ ,  
641  $FC_{HS} > 1.5$ ). Mean mutant fold-change in ideal growth ( $FC_{Growth}$ ) is superimposed as  
642 a bar plot (gray,  $FC_{Growth} < 1.0$ ; blue,  $FC_{Growth} > 1.0$ ). Mutants performing poorly in  
643 both screens (yellow;  $n = 91$ ,  $FC_{HS} < 0.5$ ,  $PFS_{HS} > 0.25$ ) were classified as HS- and  
644 Growth-Sensitive and were not considered further. Mutations neither HS-Sensitive nor  
645 HS-Tolerant were classified as HS-Neutral (taupe,  $n = 543$ ). The distribution patterns

646 between intergenic regions and CDS is almost equal comparison of pilot-library and 1K-  
647 library that demonstrate the random nature of the *pB*-mutant library (Fig. S6A-C). We  
648 checked reproducibility and validate the performance of the 1K- library by comparing  
649 correlation of the *pB*-mutants that appeared multiple times (i.e., at least twice) in different  
650 pools (Fig. S7A-B). In addition to the HS-Sensitive mutant PB4 (DHA, dynein,  
651 PF3D7\_1122900) from the pilot library, we identified three HS-Sensitive dynein mutants  
652 in the 1K-library (two different mutants of DHA\_12, PF3D7\_1202300; one mutant of  
653 DHA\_10, PF3D7\_1023100), indicating the robusticity of the 1K-library screen (Fig. S8A-  
654 B). Distributions of PFS<sub>HS</sub> for mutant HS-phenotype classifications are provided in Fig.  
655 S9.

656 **B.** Functional enrichment of GO terms for HS-Sensitive or Growth-Sensitive *pB*-mutants  
657 vs all other mutants in the 1K-library. HS-Sensitive mutants were enriched in terms  
658 associated with HS-response such as protein-folding, response to DNA-damage, DNA-  
659 repair, and regulation of vesicle-mediated transport. Growth-Sensitive mutants tended to  
660 be enriched for more general categories broadly important for survival in all conditions,  
661 such as translation- or mRNA-metabolism-related terms. Circles represent GO category,  
662 circle color represents ontology, and circle size represents number of significant genes  
663 annotated to that category. Significant terms (Fisher/elim-hybrid test *p*. value  $\leq 0.05$ )  
664 fall within the light-green box.

665

666 **Figure 3. Unfolded protein response, apicoplast-targeted and mitochondria-**  
667 **targeted stress-response pathways are critically dysregulated in functionally**  
668 **unrelated HS-Sensitive mutant clones.**

669 **A.** Genes were classified based on their NF54-expression with and without HS-exposure  
670 across all three parasite lines (Table S3, Methods). Genes identified as differentially  
671 expressed in response to febrile temperatures vs. 37°C were classified into three

672 different categories based on direction of response in the wildtype parasite NF54:  
673 upregulated in response to HS (FC-HS > 1 and FDR < 0.1; ↑ n=415), down-regulated in  
674 response to HS (FC-HS < -0.5 and FDR < 0.1; ↓ n=611), or not regulated by HS (-0.5 <  
675 FC-HS < 1; – n=1541), with upregulated genes considered to be driving the HS-  
676 response. Genes expressed above threshold in NF54 and both HS-Sensitive mutants (n  
677 = 1298) were then assigned into six HS expression-categories based on phenotype in  
678 NF54 vs. mutants  $\Delta LRR5$  and  $\Delta DHC$ . HS-regulated genes shared between NF54 and  
679 both mutants are indicated in red (↑↑↑, n = 94) or blue (↓↓↓, n = 205) for up- and down-  
680 regulated genes, respectively. Genes dysregulated in one or both HS-Sensitive mutants  
681 fell into two main expression-profile categories underlying mutant HS-Sensitivity  
682 phenotypes: those upregulated in NF54 that failed to be regulated in the mutants (↑××, n  
683 = 83), and genes not regulated in response to HS in NF54 that were inappropriately  
684 upregulated in the mutants (– ↑↑, n=74). Most remaining genes were not regulated in  
685 response to HS in any parasite line (n = 615).

686 **B.** Functional enrichment analyses between wildtype/mutant HS-expression profiles as  
687 defined in A. Red: Shared upregulated HS-responsive GO-terms between NF54 and the  
688 two HS-Sensitive *pB*-mutants (↑↑↑). Blue: Shared down-regulated HS-responsive GO-  
689 terms (↓↓↓). Ochre: GO-terms upregulated in NF54 but dysregulated in the two *pB*-  
690 mutant (↑××). Tan: GO-terms enriched in genes not regulated in the wildtype HS-  
691 response but upregulated in the mutants (– ↑↑). Only enriched GO-terms are shown  
692 (Fisher/elim-hybrid test p. value ≤ 0.05), with highest significance indicated in dark  
693 green. Fraction of significant genes mapping to a GO-term in an HS expression-profile  
694 category vs. genes mapping to that GO-term in the entire analysis is indicated by  
695 distance to the center of the circle, with the outermost position on the circle indicating  
696 100% of genes in that GO-term are significant. See Table S3D.

697 **C.** Several apicoplast and isoprenoid biosynthesis-related genes have a tendency to be  
698 upregulated in the wildtype-response to HS and are dysregulated in one or both HS-  
699 Sensitive *pB*-mutant clones (↑↗↘). \* Isoprenoid biosynthesis-related genes upregulated  
700 by HS confirmed in the pooled HS-Screen.

701

702

703 **Figure 4. Apicoplast isoprenoid biosynthesis is critical for *P. falciparum* survival**  
704 **of febrile temperatures. A.** Apicoplast-targeted genes tend to be increased in response  
705 to HS as compared to all non apicoplast-targeted genes detected above threshold in  
706 RNAseq. Apicoplast-targeted genes are as defined in <sup>47</sup> (\*\*\*) Fisher-test p-value < 1e-5,  
707 39 up- vs.12 down-regulated genes, compared with whole genome 415 up- vs. 611  
708 down-regulated genes, Fisher test p< 1e-5, Table S4A-B).

709 **B.** Apicoplast-targeted genes tend to be highly essential during blood-stage vs. all other  
710 non-apicoplast-targeted genes detected above threshold in RNAseq. The lower  
711 Mutagenesis Index Score (MIS) represents higher essentiality <sup>6</sup>, the median MIS for  
712 apicoplast-targeted genes is much lower than median MIS for all other genes, indicating  
713 a lower tolerance for disruption and thus higher likely essentiality during blood-stage  
714 development than non-apicoplast-targeted genes (\*\*\*\* Wilcoxon-test p-value < 1e-15).

715 **C.** Apicoplast pathways regulated in response to HS. GO categories enriched in up- and  
716 down-regulated apicoplast genes are shown on a scale from red to blue, respectively.  
717 The horizontal direction indicates the log ratio between up- and down-regulated  
718 apicoplast genes in each category. Circle-size represents gene-number per category.

719 **D.** All nine *pB*-mutants in genes related to apicoplast isoprenoid biosynthesis  
720 represented in the 1K-library pooled screen were HS-Sensitive. Mutants are ranked by  
721 phenotype from HS-Sensitive (red) to HS-Tolerant (green). Circles indicate each HS-  
722 Sensitive mutant related to isoprenoid-biosynthesis. \*The three isoprenoid biosynthesis-

723 genes we identified as directly upregulated in response to HS via RNAseq (DXS,  
724 PF3D7\_1337200; tRNA m(1)G methyltransferase, PF3D7\_1119100; apicoplast RNA  
725 methyltransferase, PF3D7\_0218300). See Table S3.

726 **E.** Key enzymes in the *P. falciparum* isoprenoid biosynthesis-pathway are up-regulated  
727 in response to heat-shock (red circle), dysregulated in HS-Sensitive mutants (ochre) and  
728 absent in malaria-parasites of hosts that do not present fever. Pathway diagram  
729 modeled from <sup>48</sup>. Isoprenoid biosynthesis-genes upregulated in HS include DXS, 2-C-  
730 methyl-D-erythritol 2,4-cyclodiphosphate synthase (IspF, PF3D7\_0209300), pyruvate  
731 kinase II (PyKII, PF3D7\_1037100), phosphoenolpyruvate/phosphate translocator (PPT,  
732 PF3D7\_0530200), triosephosphate isomerase (TIM, PF3D7\_1439900), triose phosphate  
733 transporter (TPT, PF3D7\_1218400), and upstream-regulator of MEP-pathway substrates  
734 HAD1-phosphatase (HAD1, PF3D7\_1033400) <sup>49</sup>. All direct downstream-targets  
735 prenylated by bifunctional farnesyl/geranylgeranyl diphosphate synthase  
736 (FPPS/GGPPS, PF3D7\_1128400) with products of the MEP-pathway (zigzag)  
737 represented in pooled screening were HS-Sensitive, including the Rab-family vesicular  
738 trafficking-proteins (Rab5c, PF3D7\_0106800; Rab7, PF3D7\_0903200; Rab11b,  
739 PF3D7\_1340700), as were several digestive vacuole proteases and proteins involved in  
740 hemoglobin digestion (PM1, PF3D7\_1407900; ATCase, PF3D7\_1344800; M1AAP,  
741 PF3D7\_1311800; LAP, PF3D7\_1446200; HSP70, PF3D7\_0818900). The key thiamin-  
742 synthesis enzyme hydroxyethylthiazole kinase (ThzK, PF3D7\_1239600) is absent in *P.*  
743 *berghei* and *P. yoelii*, malaria-parasites whose rodent-hosts do not present fever.

744 **F.** *P. falciparum* genes with plant orthologs (green circles) indicating potential  
745 endosymbiont-ancestry tend to be increased in response to HS vs. genes that do not  
746 have plant orthologs (grey circles). *P. falciparum* genes with potential endosymbiont-  
747 ancestry were derived from 1919 ortholog-pairs between *Arabidopsis thaliana* and *P.*

748 *falciparum* (data from OrthoMCLv5.0). The listed processes are sorted based on the  
749 ratio of “green” to “non-green” orthologs.

750

751 **Figure 5. Increased sensitivity to fever is directly correlated with increased**

752 **sensitivity to artemisinin in the malaria parasite. A.** HS-Sensitive *pB*-mutants (red)

753 are more sensitive to multiple concentrations of artemisinin derivatives Artesunate (AS)

754 and Dihydroartemisinin (DHA), proteasome-inhibitor Bortezomib (BTZ), and conditions of

755 heightened oxidative stress than HS-tolerant parasites (green) in all pooled screens of

756 the pilot library. HS-Sensitive mutants tended to be sensitive to both artemisinin

757 derivatives and H<sub>2</sub>O<sub>2</sub>-induced oxidative stress, while HS-Tolerant mutants were less

758 sensitive to either condition. Also, HS-Sensitive mutants shared an increased sensitivity

759 to the proteasome inhibitor BTZ (Table S5, Fig. S2, Methods). *pB*-mutants were cultured

760 continuously under oxidative stress-inducing conditions for three to six cycles (T1 and

761 T2, respectively). Samples were collected from all parallel phenotype-screens of the

762 pilot-library in biological duplicate. Biological replicates were highly correlated for each

763 screen (Pearson correlation > 0.94; Fig. S2 and S10). Mutants in apicoplast-targeted

764 genes (n = 5) have phenotypes similar to all HS-Sensitive mutants (n =28) in artemisinin-

765 derivative screens, but not to protein-inhibitors or oxidative stress (\* Wilcoxon p < 0.05;

766 \*\*\* Wilcoxon p < 1e-10. See Methods).

767 **B.** Correlation between mutant phenotypes in all pooled screens of the pilot library.

768 Mutants performing in the bottom 25% or top 25% of each screen were classified as

769 having “Sensitive” and “Tolerant” phenotypes, respectively. Mutant classifications were

770 compared pair-wise between each screen, with mutants falling into the same category in

771 both screens considered to have correlating phenotypes.

772 **C.** Compared with HS-Tolerant genes, the mRNA levels of HS-Sensitive genes are

773 significantly positively correlated with parasite clearance half-life under artemisinin-

774 based combination therapy (ACT) in field-isolates<sup>10</sup>. The red violin plot indicates 29 HS-  
775 Sensitive *pB*-mutants, while the green violin plot represents 16 HS-Tolerant mutants (\*  
776 Wilcoxon p-value < 0.05).

777 **D.** Under HS stress, genes classified as up-regulated in response to heat-stress are  
778 significantly positively correlated with parasite clearance half-life under artemisinin-  
779 based combination therapy (ACT) in field-isolates<sup>10</sup>. Down-regulated genes are more  
780 likely to be negative correlated with parasite clearance half-life. The red violin plot  
781 indicates 67 genes upregulated in WT during HS, while 114 genes are down-regulated  
782 (\*\* Wilcoxon p-value < 1e-3).

783 **E.** Both K13-mediated mechanisms of artemisinin resistance (endocytosis, ubiquitin-  
784 proteasome system) are similarly regulated in HS. The K13-defined endocytosis  
785 pathway (shades of green) and key ubiquitinating-enzymes of the ubiquitin-proteasome  
786 system, E2/E3 and K13, are downregulated in the wildtype NF54 HS-response, while  
787 protein folding, stress, exported proteins, and proteasome genes are upregulated.  
788 RNAseq data are plotted for each gene by average log<sub>2</sub> fold-change in response to  
789 HS and significance (-log<sub>2</sub>(p-value)). Circles in shades of blue and pink indicate genes  
790 significantly down- or upregulated after exposure to HS, respectively.

791 **F.** Proposed model integrating key pathways underlying the parasite survival of host  
792 fever-response and artemisinin resistance identified via pooled phenotypic screening.  
793 Direction of regulation in response to HS is informed by comparative RNAseq data  
794 where available (pink = increased; blue = decreased). Pathways/proteins previously  
795 identified as interacting with K13 are indicated (green triangle). See Tables S4C-D for  
796 data and additional supporting references.

797

## 798 **Methods**

799 *Pilot-library of pB-mutant clones characteristics and validation*

800 The single *piggyBac*-transposon insertion sites of each *pB*-mutant-clone in the pilot-  
801 library were verified as previously described <sup>13, 14</sup>, published data showed that growth  
802 rates of individual *pB*-mutant clones were highly reproducible between biological  
803 replicates, and even between pools with different compositions. All of those 128  
804 extensively characterized *P. falciparum* *pB*-mutant clones in the pilot-library were  
805 repeatedly confirmed in subsequent growth screens in 12 asexual intra-erythrocytic  
806 development cycles (24 days), bio-rep samples were collected in subsequent cycles at  
807 3, 6, 9 and 12. Additionally, whole-genome sequencing performed on 23% of 128 *pB*-  
808 mutant-clones in the pilot-library verified that no major genomic changes occurred aside  
809 from the *piggyBac* insertion, ensuring any detected phenotypes are attributable to the  
810 single disruption <sup>15</sup>. The pilot-library was generated in a manner to ensure approximately  
811 equal representation of each of the 128 clones at thaw <sup>13</sup>.

812

#### 813 *Generating the pilot-library of pB-mutant parasite clones*

814 The pilot-library was built as described in our previous QIseq methods-development  
815 study <sup>13</sup> and data are available in PlasmoDB (RRID:SCR\_013331). Aliquots of the pilot-  
816 library were generated by first growing each of the 128 extensively-characterized  
817 mutant-clones individually in T25-flasks to 1-2% parasitemia. All clones were then  
818 combined equally into one large flask and gently mixed. One-hundred equal-volume  
819 aliquots of the pilot-library were then cryopreserved according to standard methods,  
820 providing enough biological-replicate samples for use in the parallel phenotype screens  
821 of the pilot-library.

822

#### 823 *Pooled-screen assay-design*

#### 824 *HS-screens*



825 The pooled phenotypic screen-design pipeline has three important steps to ensure  
826 quality-control and scalability: 1) protocols are tested using individual *pB*-mutant clones;  
827 2) methods are adapted for pooled-screening using the well-characterized pilot-library;  
828 3) methods developed using the pilot-library are applied to 1K-library screens (Fig. S1).  
829 We exposed pools of *pB*-mutant parasites to three rounds of temperature-cycling to  
830 simulate the cyclical pattern of fever characteristic of human malaria (Figure 1A).  
831 Parasites under phenotypic selection (heat-shock) and ideal-growth controls originated  
832 from the same thaw, grown at 37°C for one cycle then split equally into five flasks (three  
833 flasks A, B and C for exposure to heat-shock, samples were harvested from these three  
834 flasks at same time as three technical-replicates for HS-Screens; two flasks C and D for  
835 the ideal-growth controls). Experimental and control-flasks were maintained in parallel to  
836 minimize potential batch-effects. Parasites were grown for one cycle at 37°C until they  
837 reached the ring-stage of development (Time-point 0;  $T^0$ ), at which point the  
838 experimental-group were exposed to febrile temperatures (41°C) for 8 hours. Post-heat-  
839 shocked parasites were then returned to 37°C for the remainder of the 48-hour window  
840 until they again reached ring-stage. Parasite-gDNA was harvested for QIseq after two  
841 more rounds of temperature-cycling in successive growth cycles to ensure enough  
842 parasite-material was available for QIseq (Time-point 1;  $T^1$ ). Control-parasites were  
843 harvested for gDNA before and after three cycles of pooled growth at 37°C ( $T^0$  and  $T^1$ ,  
844 respectively) for quantification via QIseq in technical triplicate. We used QIseq-reads  
845 obtained for each mutant after the same number of cycles of pooled growth at 37°C as  
846 our  $T^0$  control as previously reported<sup>13</sup>. Pilot-library screens were performed in biological  
847 duplicate. As the 1K-library consists of multiple randomly selected, uncloned, large  
848 mixed-population pools and direct biological replication is not feasible, we leveraged  
849 insertions duplicated across pools as internal controls. FC-HS for 15 insertion-sites  
850 represented in at least two different pools of the 1K library allowed evaluation of

851 consistency across pools. FC-HS was highly correlated between duplicate insertion-sites  
852 regardless of the pool in which they were screened (Pearson correlation = 0.806; Fig.  
853 S7A-B). We further evaluated reproducibility between the pilot library and the 1K library  
854 using mutants in genes represented in both the pilot library and the 1K-library (n = 16  
855 genes; max distance between pilot-library and 1K-library insertion < 1 kb). FC-HS was  
856 again highly correlated across pools (Fig. S8A-B, Pearson correlation = 0.702).

857

#### 858 *Drug-screens*

859 As with the HS-screen, parasites were split from the same thaw of the pilot-library after  
860 one cycle of growth into experimental flasks and control-flasks. Experimental flasks were  
861 exposed to three cycles of continuous drug-pressure at two different concentrations  
862 (IC10, IC25) of each artemisinin-compound (AS, DHA). Proteasome-inhibitor BTZ-  
863 experiments were performed at IC10. Control-flasks were cultured continuously in  
864 parallel at 37°C without drug. Parasites were harvested immediately at the conclusion of  
865 three growth-cycles for gDNA-extraction and phenotype-analysis via QIseq.

866

#### 867 *Oxidative stress screens*

868 Parasites were split after one cycle of growth from the same thaw of the pilot-library as  
869 the HS-screen. Parasites were grown one more cycle, then split into four flasks: two  
870 control-flasks to be cultured with standard, washed human red blood-cells (hRBC), and  
871 two experimental flasks to be cultured with H<sub>2</sub>O<sub>2</sub>-treated hRBCs to mimic conditions of  
872 oxidative stress. Experimental flasks (H<sub>2</sub>O<sub>2</sub> treated-hRBC) and control-flasks (untreated-  
873 hRBC) were cultured continuously in parallel at 37°C. Parasites were harvested  
874 immediately after three growth-cycles (T1), then again after an additional three growth-  
875 cycles (T2) for gDNA-extraction and phenotype-analysis by QIseq.

876

877 Methods for oxidative pre-treatment of hRBCs were as published previously<sup>50</sup>. Briefly,  
878 O+ hRBCs (Interstate blood bank, packed, 100% hematocrit) were incubated with 1 mM  
879 H<sub>2</sub>O<sub>2</sub> (Sigma-aldrich, Cat. no. H1009-100ML) for one hour at room temperature. After  
880 treatment, cells were washed three times with phosphate-buffered saline (PBS) before  
881 dithiothreitol (DTT) was added to a final concentration of 1 mM to heal any reversible  
882 oxidative damages. Cells were then treated with menadione sodium bisulphite for one  
883 hour at room temperature (Sigma-aldrich Cat. no. M5750-100G) and washed five times.  
884 A volume of 3–4 ml of AB medium (RPMI 1640 medium supplemented with 2 mM L-  
885 glutamine, 25 mM HEPES, 100 µM hypoxanthine and 20 µg ml<sup>-1</sup> gentamicin) was added  
886 on top of the cell-pellet after discarding the final wash. Pre-treated erythrocytes were  
887 stored at 4 °C before use in parasite culture.

888

889 All pooled phenotypic screens of pilot-library (AS, DHA, BTZ, oxidative stress, ideal  
890 growth) were performed in biological duplicate (Fig. S10).

891

892 *Qlseq*

893 Qlseq, which uses Illumina next-gen sequencing technology and custom library-  
894 preparation to enable sequencing from both the 5' and 3' ends of the *piggyBac*  
895 transposon out into the disrupted genome-sequence, allows quantitative identification of  
896 each *pB*-mutant line by its unique insertion-site within mixed-population pools of *pB*-  
897 mutants<sup>13</sup> (Figure 1B). The anatomy of the *piggyBac* transposon and its distinct 5' and 3'  
898 inverted terminal-repeat sequences (ITRs) allows double-verification of insertion-sites;  
899 both 5' and 3' Qlseq libraries were therefore generated and sequenced for each sample.  
900 Counts per insertion-site were determined as described previously<sup>13</sup>. We observed high  
901 correlation between biological replicates at 41C and 37C respectively (Pearson  
902 correlation = 0.964 at 41C and 0.967 at 37C, Fig. S5A). We observed lower correlation

903 between Growth (37C) and HS (41C) assays (Fig. S5B, average Pearson correlation =  
904 0.723), suggesting that our heat-shock exposure-conditions are sufficient to allow  
905 reproducible detection of mutants with specific selection response-phenotypes from  
906 pooled screening.

907

908 *Calculating mutant fold-change in pooled screening to assign HS- and Growth-*  
909 *phenotypes*

910 We defined FC-Growth by *pB*-mutant fold-change after three cycles of growth at ideal  
911 temperatures ( $T^{1-37C} / T^{0-37C}$ ). FC-HS was defined as *pB*-mutant fold-change after  
912 exposure to heat-shock vs. the non- heat-shocked control ( $T^{1-41C} / T^{1-37C}$ ). We used  
913 changes in reads-number detected for each *pB*-mutant in the Growth-Screen and the  
914 HS-Screen as compared to reads-number detected for that mutant in the respective  
915 control-screen to calculate mutant Fold Change (FC) in both screens (Figure 1C-D;  
916 Methods). We then ranked mutants from lowest to highest FC, with lowest FC indicating  
917 highest sensitivity to the screened-condition.

918

919 We developed a scoring-system to distinguish mutants with phenotypes specifically in  
920 the condition under selection (HS) vs. those with inherently compromised growth in ideal  
921 conditions, called the Phenotypic Fitness-Score (PFS).  $PFS_{HS}$  is the mutant fold-change  
922 in response to heat-shock (FC-HS, 41C/37C) multiplied by the ratio of FC-HS to mutant  
923 fold-change under ideal growth-conditions (FC-HS/FC-Growth), with the smallest and  
924 largest values indicating the largest mutant growth-differentials between the two screens  
925 (smallest  $PFS_{HS}$  indicating worse mutant-fitness in the HS-Screen than the Growth-  
926 Screen, and largest  $PFS_{HS}$  indicating better mutant-fitness in the HS-Screen than the  
927 Growth-screen). Mutants exhibiting (1) poor growth in the HS-Screen (i.e., low FC-HS of  
928  $< 0.5$  based on performance of \*known HS-Sensitive *pB*-mutant-clones), and (2)

929 comparatively much better growth in the Growth-Screen (i.e., low  $PFS_{HS}$  of  $< 0.25$ ) were  
930 classified as HS-Sensitive in pooled phenotypic screens (indicated in red in Fig. 1E-F).  
931 Mutants exhibiting poor fitness in both the Growth- and HS-Screens ( $FC_{HS} < 0.5$  and  
932  $PFS_{HS} > 0.25$ ) are indicated in Fig. 1E-F in yellow ( $n = 14$ ). These double-sensitive  
933 mutants were not included in our “HS-Sensitive” classification to avoid overinterpretation  
934 of possibly-confounding phenotypes. We classified mutants displaying a slight growth  
935 advantage in response to heat shock ( $FC_{HS} > 1.5$ ,  $n = 28$ , indicated in the green box,  
936 Fig.1E-F) as “HS-Tolerant”. Mutants exhibiting neither sensitivity nor tolerance to heat  
937 shock were classified as HS-Neutral ( $n = 49$ ).

938

#### 939 *Assigning drug- and oxidative stress-screen phenotypes*

940 Mutant fold-change in response to the given condition was calculated against an ideal-  
941 growth control as above. Mutants in the top 25% of reads recovered in QIseq in the  
942 screened condition were classified as Tolerant, while mutants in the bottom 25% were  
943 classified as Sensitive.

944

#### 945 *Comparative RNAseq between wild-type NF54 and two HS-Sensitive mutant parasite* 946 *lines in response to heat shock*

947 RNAseq experimental design is outlined in Fig. S11A. Briefly, highly synchronized ring-  
948 stage cultures of wildtype NF54 and HS-Sensitive mutants *LRR5* and *DHC* were split  
949 equally into four T75 flasks each. All parasites were grown at the normal human body  
950 temperature (37C) to early ring-stage. Two flasks of each parasite-line were then  
951 exposed to febrile temperatures (41C) for 8 hours, while the remaining two flasks were  
952 allowed to continue to grow at 37C for 8 hours without exposure to heat-stress. This  
953 temperature-cycling was repeated three times, just as we allowed for the pooled HS-  
954 Screen. After the third round of heat-shock (Time 1,  $T^1$ ), RNA was harvested

955 simultaneously from both conditions for RNAseq as in <sup>19</sup>. Parasite fold-change in  
956 response to HS was calculated at the time of sample-collection and verified mutant  
957 defects in response to HS as compared to NF54 (Fig S8B). RNA-seq was performed in-  
958 house on an Illumina MiSeq using a 300-cycle V2 MiSeq reagent kit.

959

#### 960 *RNA-seq data-analysis*

961 RNA-seq reads from each sample were aligned to the *P. falciparum* reference genome  
962 (PlasmoDB version 28, RRID:SCR\_013331). A maximum of one mismatch per read was  
963 allowed. The mapped reads from TopHat <sup>51</sup> were used to assemble known transcripts  
964 from the reference and their abundances were estimated using Cufflinks <sup>52</sup>. The  
965 expression level of each gene was normalized as FPKM (fragments per kilobase of exon  
966 per million mapped reads). We defined expressed genes as those having FPKM > 20 for  
967 at least one biological replicate at either 37°C or 41°C. The fold change of normalized  
968 gene expression between 41°C and 37°C was calculated for every biological replicate.  
969 Fold-change for genes not expressed in both temperatures was set equal to one. We  
970 conservatively filtered out genes in the top and bottom 10% of fold-change to remove  
971 outliers. We then fit a Gaussian model to the log<sub>2</sub> fold change (*log<sub>2</sub>FC*) for every  
972 biological replicate using maximum log likelihood estimation to assess the fold-change  
973 distribution. The p-value is calculated as the probability of estimated gaussian distribution  
974 higher than the observed *log<sub>2</sub>FC* (when observed *log<sub>2</sub>FC* > the expectation of estimated  
975 gaussian distribution), or lower than the observed *log<sub>2</sub>FC* (when observed *log<sub>2</sub>FC* ≤ the  
976 expectation of estimated gaussian distribution). The false discovery rate (FDR) was  
977 calculated for each replicate. We defined genes for which FDR < 0.1 in both biological  
978 replicates as having significant fold-change in response to HS. Genes were assigned HS  
979 phenotype-categories based on significance and direction of HS-response. We assigned  
980 HS phenotype-categories for 2567 genes using these criteria (Table S3). Heat-shock

981 phenotypes as identified via pooled phenotypic screening and comparative RNAseq  
982 were highly correlated (Fig. S12A-B), supporting our methodology.

983

#### 984 *GO-term enrichment analyses*

985 All GO-enrichment analyses were performed testing GO-terms mapped to genes in the  
986 category of interest against a background of GO-terms mapped to all other genes in the  
987 analysis. The GO-term database was created from the latest curated *P. falciparum*  
988 ontology available at the time of analysis, downloaded from GeneDB (accessed May 2,  
989 2019)<sup>53</sup>. For enrichment-analysis in the 1K-library screens: Mutants were divided into  
990 HS-phenotype categories, and each category was tested for enrichment against a  
991 background of GO-terms mapped to the genes represented by the remainder of the 922  
992 mutants in the screen using the weighted Fisher/elim hybrid-method of the TopGO  
993 package (v 1.0) available from Bioconductor<sup>54</sup> (Fig. 2B). For enrichment-analysis in  
994 comparative RNAseq data: a database of all GO-terms mapped to the 1298 genes which  
995 could be assigned a HS-phenotype in all three parasites was assembled. Genes were  
996 divided into HS phenotype-categories based on direction of fold-change (Up, Down,  
997 Unchanged) in response to HS in all three parasites, then evaluated for GO-term  
998 enrichment against the background GO-term database of all other genes in the analysis  
999 using the weighted-Fisher/elim hybrid-method of the TopGO package (Fig 3B, Table  
1000 S3B-D). For enrichment of apicoplast-targeted genes by RNAseq HS-phenotype  
1001 category: enrichment for each investigated GO-term  $g$  (The x-axis in Fig 4c, the ratio of  
1002 up to down regulated genes) was calculated as the ratio ( $C_g$ ) of up- vs. down-regulated  
1003 genes mapped to GO-term  $g$  among all differential expressed apicoplast genes. This  
1004 ratio ( $C$ ) was also calculated for the genes mapped to GO-term  $g$  in the whole genome  
1005 (the background distribution). The GO annotation for each gene was downloaded from  
1006 GeneDB (accessed May 2, 2019). The fraction of HS-regulated apicoplast-genes to

1007 non-HS-regulated apicoplast genes ( $C_r/C$ ) was assessed for significance using the  
1008 Fisher exact test (Fig 4C; Table S4A-B).

1009

## 1010 **SUPPLEMENTARY FIGURE and TABLE LEGENDS**

1011 **Figure S1. Schematic overview of the phenotypic screening pipeline.**  $pB$ -mutant  
1012 library resources from small (individual, well-characterized mutant-clones) to large (the  
1013 1K-Library, comprised of pools randomly selected from the Saturation-Library) were  
1014 used to design carefully validated pooled screens at increasingly large scale. 1) to test  
1015 the protocols using individual  $pB$ -mutant clones; 2) to develop pooled phenotypic screen  
1016 method using pilot-library screen; 3) then we scale-up phenotypic screen using 1K-  
1017 library; 4) parallel phenotype screens using pilot-library; 5) Transcriptional profiling via  
1018 RNAseq compare the parasite response to heat shock between the wildtype and HS-  
1019 sensitive mutants. High correlation between mutant-phenotypes in HS-screens and  
1020 ART-screens indicated mechanistic overlap in response to both stressors. Iterative  
1021 rounds of pooled-screening for various phenotypes over time enables higher-throughput  
1022 functional-annotation of the *P. falciparum* genome.

1023

## 1024 **Figure S2. Extended screening data against the pilot-library and summary.**

1025 **A.** Full drug-screening data for artemisinin-compounds AS and DHA, and proteasome-  
1026 inhibitor Bortezomib (BTZ) against the pilot-library. HS-Sensitive mutants are  
1027 significantly more sensitive to each drug than HS-Tolerant mutants. There is no  
1028 significant relationship between  $pB$ -mutant sensitivity to any drug and mutant sensitivity  
1029 in standard growth-conditions.

1030 **B.** HS-Sensitive (red) and HS-Tolerant (green) mutants and their phenotypes across all  
1031 pooled phenotypic screens. Mutants are clustered by HS-phenotype.

1032



1033 **Figure S3. Mutants in members of the DV proteome, targets of ART alkylation, and**  
1034 **putative interacting partners of K13 tend to be sensitive to HS.**

1035 **A.** 1k HS-Screen mutants are ordered by FC-HS from HS-Sensitive to HS-Tolerant.

1036 Mutants in digestive vacuole-associated proteins as defined by [26] are indicated in  
1037 lavender dots. Gene-symbols for mutants with HS-sensitivity are labeled with black text  
1038 (10 of 18 genes). Gene-symbols for HS-Neutral and HS-Tolerant mutants are labeled  
1039 with grey text.

1040 **B.** All mutants in ART alkylation-targets as defined by <sup>9</sup> included in the 1K HS-Screen.

1041 **C.** HS-screen phenotypes of mutants in putative K13-interacting proteins as defined by  
1042 <sup>25</sup>.

1043

1044 **Figure S4. A. Core proteasome-components are slightly but universally**

1045 **upregulated in response to HS** as compared to other aggregatedly upregulated  
1046 processes which have more heterogenous expression. Fold-change for most individual  
1047 proteasome-components did not meet our threshold to be designated “upregulated”. \*\*  
1048 Wilcoxon p-value < 1e-5.

1049 **B. Activation of pathways underlying DHA-mediated killing and febrile-**

1050 **temperature survival is directly inverse. Top.** Model of DHA-mediated killing in *P.*

1051 *falciparum* adapted from <sup>8</sup>. Artemisinin (ART) damages and unfolds proteins, prevents  
1052 folding of newly synthesized proteins, and inhibits the proteasome while at the same  
1053 time activating E1/E2/E3 ubiquitin-machinery. Accumulation of toxic polyubiquitinated  
1054 protein-substrates (S) overwhelms the cell and leads to death. **Bottom.** Model of

1055 parasite fever-response. Heat-stress causes globally damaged protein. The

1056 parasite increases the UPR as it inhibits E2/E3 ubiquitination to prevent accumulation of

1057 toxic, polyubiquitinated (Ub) protein-aggregates, while at the same time increasing its

1058 capacity for proteasome-mediated degradation—ultimately enabling the parasite to  
1059 resolve heat-shock-instigated stress and survive febrile-temperatures.

1060

1061 **Figure S5. QIseq data-correlations within and between Pilot-Library Screens.**

1062 **A.** Pearson correlations between 5' and 3' QIseq data for 37°C\_ideal-growth screen and  
1063 41°C\_heat-shock screen indicate highly reproducible analyses across technical and  
1064 biological replicates in both screens (Figure 1B).

1065 **B.** Correlations within and between 37°C\_ideal growth screen and 41°C\_heat-shock  
1066 screen QIseq data. The samples were collected in HS-Screens of the pilot-library include  
1067 two bio-reps and three technical-reps (Figure 1A; Method, HS-Screen). High correlations  
1068 of two bio-reps within both HS-screens and Growth-screens (HS-Screen,  $R=0.94$ ;  
1069 Growth-Screen,  $R=0.89$ ) indicate the pilot-library screens are highly reproducible, and  
1070 weak correlation between HS-screens and Growth-screens ( $R = \sim 0.42$ ) suggests heat-  
1071 shock exposure-conditions were sufficient to allow reproducible detection of mutants  
1072 with specific selection response-phenotypes from pooled screening.

1073

1074 **Figure S6. *pB*-mutant insertions are randomly distributed in the pilot-library and  
1075 the 1K-library.**

1076 **S6A.** Comparative analysis of the *piggyBac* mutants' distribution patterns in coding vs  
1077 noncoding regions between the pilot-library and 1K-library. Distribution patterns between  
1078 intergenic regions and CDS are almost equal, with composition also reflecting the  
1079 distribution of the saturation mutagenesis-library as a whole<sup>6</sup>.

1080 **S6B.** *pB*-mutants' distribution patterns across HS phenotype-categories of the 1K library.  
1081 HS-Tolerant mutants were more likely associated with dispensable genes (genes with  
1082 exonic insertions) than HS-Sensitive genes.

1083 **S6C.** Distances between insertions of the 1K library are random. There is no significant  
1084 difference in distance between each pair of neighboring *piggyBac* insertions of the 1K  
1085 library and coordinates chosen by random sampling (p-value = 0.787, Mann-Whitney U  
1086 test). Sampling was repeated 100x with sites randomly selected across all  
1087 chromosomes.

1088

1089 **Figure S7. Reproducibility of the 1K-library HS-Screen.**

1090 **A.** The 1K-library consists of randomly selected, uncloned large mixed-population pools  
1091 (LMPP) of ~100 unique mutants per pool. Fifteen insertion-sites are duplicated in  
1092 mutants of at least one other pool. Each of the 12 LMPP comprising the 1K-library  
1093 (LMPP\_1-6; LMPP\_10-15) are indicated on the x-axis with violin plots showing the  
1094 distribution of mutant fold change in response to heat shock (FC-HS) within that pool.  
1095 FC-HS of the fifteen insertion-sites duplicated in at least one other pool are plotted in  
1096 color, with insertion location-category indicated by shape.

1097 **B.** FC-HS of duplicated insertional mutants are highly correlated across pools (Pearson  
1098 correlation = 0.806), indicating high reproducibility of mutant phenotypes independent of  
1099 mutant pool-composition. Insertions are represented as in plot A.

1100

1101 **Figure S8. Reproducibility within and between the pilot-library and 1K-library HS-**  
1102 **Screens.**

1103 **A.** Within- and between-library consistency indicates the robusticity of HS phenotype-  
1104 assignments in pooled screening. Dynein heavy chain (DHC) gene-family mutants (two  
1105 in DHA\_12, PF3D7\_1202300; one mutant of DHA\_10, PF3D7\_1023100) were  
1106 consistently identified as HS-Sensitive in the pilot-library and across multiple pools of the  
1107 1K-library, as were representatives of FIKK-family genes.

1108 **B.** Heatshock phenotypes are reproducible between the pilot library and the 1K-library.  
1109 FC-HS of insertional mutants in genes represented in both the pilot library and the 1K-  
1110 library (n = 16 genes; colored points) are highly correlated (Pearson correlation = 0.702).  
1111 Insertion coordinate in the pilot library is indicated on the left of the '|', while insertion  
1112 coordinate of the mutant in the same gene in the 1K-library is to the right. Distance  
1113 between the pilot-library insertion and the 1K-library insertion is indicated by shape  
1114 (maximum distance = 1kb).

1115

1116

1117 **Figure S9. Phenotypic Fitness-Score in HS (PFS<sub>HS</sub>) distribution across mutant HS**  
1118 **phenotype-classifications in the 1K-Library screen.** See Table S2 and Methods for  
1119 PFS<sub>HS</sub> calculation details. HS-Sensitive mutants (mutants displaying defective growth in  
1120 response to heat shock but not in response to ideal growth conditions) are assigned the  
1121 lowest PFS<sub>HS</sub>, while HS-Tolerant mutations are assigned the highest PFS<sub>HS</sub>.

1122

1123 **Figure S10. QIseq data-correlations within and between Pilot-Library phenotypic**  
1124 **screens: drugs and oxidative stress.**

1125 All pooled phenotypic screens of pilot-library (AS, DHA, BTZ, oxidative stress, ideal  
1126 growth) were performed in biological duplicate, high correlations of bio-reps indicate  
1127 highly reproducible analyses across all pilot-library phenotype screens.

1128

1129 **Figure S11. Methods and validation for comparative RNAseq.**

1130 **A.** RNA sample-collection methods for wildtype malaria-parasite NF54 vs. two HS-  
1131 Sensitive *pB*-mutant clones  $\Delta DHC$  (PB4) and  $\Delta LRR5$  (PB31) in response to febrile  
1132 temperatures. Assays were performed in biological duplicate.

1133 **B.** Validation of HS-Sensitive mutant-clones during RNA-Seq Sample preparation. Both  
1134 mutants grown individually had growth-defects in response to HS as compared to NF54.

1135

1136 **Figure S12. Complementary methods (pooled phenotypic screening, phenotypic**  
1137 **transcriptional profiling of HS-Sensitive mutants vs. wildtype in response to heat**  
1138 **stress) indicate genes driving the parasite heat-stress response.**

1139 **A.** HS-Sensitive *pB* mutants tend to have mutations in genes that have significant  
1140 changes in expression in response to heat-stress, while mutants that are neutral to or  
1141 tolerant of heat-stress tend to have mutations in genes that are not regulated in  
1142 response to heat-stress.

1143 **B.** *pB* mutants in genes normally up-regulated in response to heat-stress grow poorly in  
1144 response to heat-stress (i.e., have significantly lower phenotypic fitness-scores ) than  
1145 mutants in genes that are neutral or down-regulated in response to heat-stress.

1146

1147 **Supplemental Tables:**

1148 **Table S1A. Pooled HS-Screen results of the *P. falciparum* *pB*-mutant pilot-library**  
1149 **(n = 128, Fig. 1).**

1150 **S1B.** Summary counts of pilot-library mutants by phenotype-category in pooled  
1151 screening.

1152 **S1C.** GeneIDs, functional information, and distance to the insertion-site for neighboring  
1153 genes on both sides of *piggyBac* insertions of the pilot library.

1154

1155 **Table S2A. Pooled HS-Screen results of the 1K-Library (n = 922, Fig. 2).**

1156 **S2B.** Summary counts of 1K-library mutants by phenotype-category in pooled screening.

1157 **S2C.** GeneIDs, functional information, and distance to the insertion-site for neighboring  
1158 genes on both sides of *piggyBac* insertions of the 1K-library.

1159

1160 **Table S3. Comparative RNAseq-results between NF54 and HS-Sensitive mutant-**  
1161 **clones  $\Delta LRR5$  and  $\Delta DHC$  in response to heat-shock (Fig. 3).**

1162 **S3A.** All genes classified into HS response-categories in NF54 with or without exposure  
1163 to heat-shock using RNAseq data (n = 2567). HS-classifications for each gene in two  
1164 HS-Sensitive mutant-lines are indicated where available. Criteria for inclusion: NF54  
1165 expression above threshold (FPKM  $>$  or  $=$  20 for at least one replicate in at least one  
1166 temperature-condition) and FC-HS supported by two biological replicates.

1167 **S3B.** Genes included in functional enrichment-analyses. Criteria for inclusion: all genes  
1168 with expression above threshold AND agreement between replicates as to HS fold-  
1169 change classification for all three parasite lines (n = 1298).

1170 **S3C.** Enriched GO-terms for specified HS-response-categories as included in Figure 3B.  
1171 “Annotated”: the number of genes annotated to a given GO-term included in the analysis  
1172 for all HS response-categories. “Significant”: the number of genes annotated to a given  
1173 GO-term in the HS response-category being tested for enrichment.

1174 **S3D.** Full functional enrichment-results for all HS response-categories.

1175

1176 **Table S4. Apicomplast genes regulated in response to HS (Fig. 4).**

1177 **S4A.** Apicomplast-targeted genes regulated in response to HS (RNAseq data used in  
1178 Figure 4A-B).

1179 **S4B.** GO-terms mapped to HS-regulated apicomplast-targeted genes (pertains to Fig. 4C).

1180 **S4C.** Pooled heatshock-screen data for all mutants associated with processes of interest  
1181 highlighted in Figures 4D-E.

1182 **S4D.** Comparative wildtype/HS-Sensitive mutant RNAseq data for genes associated with  
1183 processes of interest highlighted in Figure 4E.

1184

1185 **Table S5. Drug- and oxidative stress-screen results of the pilot library (n = 128).**

1186 **Table S6A-B. Data pertaining to Figure 5C and 5D.**

1187 **Table S7. QIseq dataset accession numbers.**

1188

1189 **References**

1190

- 1191 1. WHO. World Malaria Report. *World Health Organization*, (2018).  
1192
- 1193 2. Gardner MJ, *et al.* Genome sequence of the human malaria parasite  
1194 *Plasmodium falciparum*. *Nature* **419**, 498-511 (2002).  
1195
- 1196 3. Aurrecochea C, *et al.* PlasmoDB: a functional genomic database for malaria  
1197 parasites. *Nucleic Acids Res* **37**, D539-543 (2009).  
1198
- 1199 4. Oakley MS, Gerald N, McCutchan TF, Aravind L, Kumar S. Clinical and  
1200 molecular aspects of malaria fever. *Trends in parasitology* **27**, 442-449 (2011).  
1201
- 1202 5. Oakley MSM, *et al.* Molecular factors and biochemical pathways induced by  
1203 febrile temperature in intraerythrocytic *Plasmodium falciparum* parasites.  
1204 *Infection and immunity* **75**, 2012-2025 (2007).  
1205
- 1206 6. Zhang M, *et al.* Uncovering the essential genes of the human malaria parasite  
1207 *Plasmodium falciparum* by saturation mutagenesis. *Science* **360**, (2018).  
1208
- 1209 7. Rocamora F, *et al.* Oxidative stress and protein damage responses mediate  
1210 artemisinin resistance in malaria parasites. *PLoS Pathog* **14**, e1006930-  
1211 e1006930 (2018).  
1212
- 1213 8. Bridgford JL, *et al.* Artemisinin kills malaria parasites by damaging proteins and  
1214 inhibiting the proteasome. *Nature Communications* **9**, 3801 (2018).  
1215
- 1216 9. Ismail HM, *et al.* Artemisinin activity-based probes identify multiple molecular  
1217 targets within the asexual stage of the malaria parasites *Plasmodium falciparum*  
1218 3D7. *Proceedings of the National Academy of Sciences* **113**, 2080-2085 (2016).  
1219
- 1220 10. Mok S, *et al.* Drug resistance. Population transcriptomics of human malaria  
1221 parasites reveals the mechanism of artemisinin resistance. *Science* **347**, 431-435  
1222 (2015).

1223

- 1224 11. Yang T, *et al.* Decreased K13 Abundance Reduces Hemoglobin Catabolism and  
1225 Proteotoxic Stress, Underpinning Artemisinin Resistance. *Cell Reports* **29**, 2917-  
1226 2928.e2915 (2019).  
1227
- 1228 12. Birnbaum J, *et al.* A Kelch13-defined endocytosis pathway mediates artemisinin  
1229 resistance in malaria parasites. *Science* **367**, 51 (2020).  
1230
- 1231 13. Bronner IFF, *et al.* Quantitative Insertion-site Sequencing (QIseq) for high  
1232 throughput phenotyping of transposon mutants. *Genome Research*, (2016).  
1233
- 1234 14. Balu B, *et al.* *piggyBac* is an effective tool for functional analysis of the  
1235 *Plasmodium falciparum* genome. *BMC microbiology* **9**, 83 (2009).  
1236
- 1237 15. Thomas P, *et al.* Phenotypic Screens Identify Parasite Genetic Factors  
1238 Associated with Malarial Fever Response in *Plasmodium falciparum piggyBac*  
1239 Mutants. *mSphere* **1**, (2016).  
1240
- 1241 16. Bushell E, *et al.* Functional Profiling of a *Plasmodium* Genome Reveals an  
1242 Abundance of Essential Genes. *Cell* **170**, 260-272.e268 (2017).  
1243
- 1244 17. Gisselberg JE, Zhang L, Elias JE, Yeh E. The Prenylated Proteome of  
1245 *Plasmodium falciparum* Reveals Pathogen-specific Prenylation Activity and Drug  
1246 Mechanism-of-action. *Molecular & Cellular Proteomics* **16**, S54-S64 (2017).  
1247
- 1248 18. Suazo KF, Schaber C, Palsuledesai CC, Odom John AR, Distefano MD. Global  
1249 proteomic analysis of prenylated proteins in *Plasmodium falciparum* using an  
1250 alkyne-modified isoprenoid analogue. *Scientific Reports* **6**, 38615 (2016).  
1251
- 1252 19. Gibbons J, *et al.* Altered expression of K13 disrupts DNA replication and repair in  
1253 *Plasmodium falciparum*. *BMC Genomics* **19**, 849 (2018).  
1254
- 1255 20. Krishnan KM, Williamson KC. The proteasome as a target to combat malaria: hits  
1256 and misses. *Translational Research* **198**, 40-47 (2018).  
1257
- 1258 21. Ng CL, Fidock DA, Bogyo M. Protein Degradation Systems as Antimalarial  
1259 Therapeutic Targets. *Trends in Parasitology* **33**, 731-743 (2017).  
1260



- 1261 22. Arie F, *et al.* A molecular marker of artemisinin-resistant *Plasmodium falciparum*  
1262 malaria. *Nature* **505**, 50-55 (2014).  
1263
- 1264 23. Tilley L, Straimer J, Gnädig NF, Ralph SA, Fidock DA. Artemisinin Action and  
1265 Resistance in *Plasmodium falciparum*. *Trends in parasitology* **32**, 682-696  
1266 (2016).  
1267
- 1268 24. Bhattacharjee S, *et al.* Remodeling of the malaria parasite and host human red  
1269 cell by vesicle amplification that induces artemisinin resistance. *Blood* **131**, 1234-  
1270 1247 (2018).  
1271
- 1272 25. Gnädig NF, *et al.* Insights into the intracellular localization, protein associations  
1273 and artemisinin resistance properties of *Plasmodium falciparum* K13. *PLoS*  
1274 *Pathog* **16**, e1008482 (2020).  
1275
- 1276 26. Lamarque M, *et al.* Food vacuole proteome of the malarial parasite *Plasmodium*  
1277 *falciparum*. *Proteomics Clin Appl* **2**, 1361-1374 (2008).  
1278
- 1279 27. Dogovski C, *et al.* Targeting the Cell Stress Response of *Plasmodium falciparum*  
1280 to Overcome Artemisinin Resistance. *PLoS Biology* **13**, e1002132 (2015).  
1281
- 1282 28. White JK, Handa S, Vankayala SL, Merkler DJ, Woodcock HL. Thiamin  
1283 Diphosphate Activation in 1-Deoxy-d-xylulose 5-Phosphate Synthase: Insights  
1284 into the Mechanism and Underlying Intermolecular Interactions. *J Phys Chem B*  
1285 **120**, 9922-9934 (2016).  
1286
- 1287 29. Imlay L, Odom AR. Isoprenoid Metabolism in Apicomplexan Parasites. *Current*  
1288 *Clinical Microbiology Reports* **1**, 37-50 (2014).  
1289
- 1290 30. Kennedy K, *et al.* Delayed death in the malaria parasite *Plasmodium falciparum*  
1291 is caused by disruption of prenylation-dependent intracellular trafficking. *PLoS*  
1292 *Biology* **17**, e3000376 (2019).  
1293
- 1294 31. Howe R, Kelly M, Jimah J, Hodge D, Odom AR. Isoprenoid biosynthesis  
1295 inhibition disrupts Rab5 localization and food vacuolar integrity in *Plasmodium*  
1296 *falciparum*. *Eukaryot Cell* **12**, 215-223 (2013).  
1297
- 1298 32. Pandey AV, Tekwani BL, Singh RL, Chauhan VS. Artemisinin, an endoperoxide  
1299 antimalarial, disrupts the hemoglobin catabolism and heme detoxification  
1300 systems in malarial parasite. *J Biol Chem* **274**, 19383-19388 (1999).  
1301

- 1302 33. del Pilar Crespo M, *et al.* Artemisinin and a series of novel endoperoxide  
1303 antimalarials exert early effects on digestive vacuole morphology. *Antimicrob*  
1304 *Agents Chemother* **52**, 98-109 (2008).  
1305
- 1306 34. Sussmann RAC, Fotoran WL, Kimura EA, Katzin AM. *Plasmodium falciparum*  
1307 uses vitamin E to avoid oxidative stress. *Parasit Vectors* **10**, 461-461 (2017).  
1308
- 1309 35. Mène-Saffrané L. Vitamin E Biosynthesis and Its Regulation in Plants.  
1310 *Antioxidants (Basel)* **7**, 2 (2017).  
1311
- 1312 36. Estévez JM, Cantero A, Reindl A, Reichler S, León P. 1-Deoxy-d-xylulose-5-  
1313 phosphate Synthase, a Limiting Enzyme for Plastidic Isoprenoid Biosynthesis in  
1314 Plants. *Journal of Biological Chemistry* **276**, 22901-22909 (2001).  
1315
- 1316 37. Zhang F, *et al.* Molecular Characterization of the 1-Deoxy-D-Xylulose 5-  
1317 Phosphate Synthase Gene Family in *Artemisia annua*. *Frontiers in Plant Science*  
1318 **9**, (2018).  
1319
- 1320 38. Heuston S, Begley M, Gahan CGM, Hill C. Isoprenoid biosynthesis in bacterial  
1321 pathogens. *Microbiology* **158**, 1389-1401 (2012).  
1322
- 1323 39. Brunetti C, Guidi L, Sebastiani F, Tattini M. Isoprenoids and phenylpropanoids  
1324 are key components of the antioxidant defense system of plants facing severe  
1325 excess light stress. *Environmental and Experimental Botany* **119**, 54-62 (2015).  
1326
- 1327 40. Mathews ES, Jezewski AJ, Odom John AR. Protein prenylation and Hsp40 in  
1328 thermotolerance of *Plasmodium falciparum* malaria parasites. *bioRxiv*, 842468  
1329 (2019).  
1330
- 1331 41. Clarke A. The thermal limits to life on Earth. *International Journal of Astrobiology*  
1332 **13**, 141-154 (2014).  
1333
- 1334 42. Kobayashi Y, *et al.* Algae sense exact temperatures: small heat shock proteins  
1335 are expressed at the survival threshold temperature in *Cyanidioschyzon merolae*  
1336 and *Chlamydomonas reinhardtii*. *Genome biology and evolution* **6**, 2731-2740  
1337 (2014).  
1338
- 1339 43. Li GQ, Arnold K, Guo XB, Jian HX, Fu LC. Randomised comparative study of  
1340 mefloquine, qinghaosu, and pyrimethamine-sulfadoxine in patients with  
1341 falciparum malaria. *Lancet* **2**, 1360-1361 (1984).  
1342

- 1343 44. Kirkman LA, *et al.* Antimalarial proteasome inhibitor reveals collateral sensitivity  
1344 from intersubunit interactions and fitness cost of resistance. *Proceedings of the*  
1345 *National Academy of Sciences* **115**, E6863 (2018).  
1346
- 1347 45. Oberstaller J, Otto TD, Rayner JC, Adams JH. Essential Genes of the Parasitic  
1348 Apicomplexa. *Trends Parasitol*, (2021).  
1349
- 1350 46. Oberstaller J, Zhang M, Wang C. RNAseq dataset: Malaria-parasite survival of  
1351 host fever is linked to artemisinin resistance ) (2020).  
1352
- 1353 47. Boucher MJ, Yeh E. Disruption of Apicoplast Biogenesis by Chemical  
1354 Stabilization of an Imported Protein Evades the Delayed-Death Phenotype in  
1355 Malaria Parasites. *mSphere* **4**, e00710-00718 (2019).  
1356
- 1357 48. Ralph SA, *et al.* Metabolic maps and functions of the *Plasmodium falciparum*  
1358 apicoplast. *Nature Reviews Microbiology* **2**, 203 (2004).  
1359
- 1360 49. Guggisberg AM, *et al.* A sugar phosphatase regulates the methylerythritol  
1361 phosphate (MEP) pathway in malaria parasites. *Nature Communications* **5**, 4467  
1362 (2014).  
1363
- 1364 50. Cyrklaff M, *et al.* Oxidative insult can induce malaria-protective trait of sickle and  
1365 fetal erythrocytes. *Nature Communications* **7**, 13401 (2016).  
1366
- 1367 51. Trapnell C, Pachter L, Salzberg SL. TopHat: discovering splice junctions with  
1368 RNA-Seq. *Bioinformatics* **25**, 1105-1111 (2009).  
1369
- 1370 52. Trapnell C, *et al.* Transcript assembly and quantification by RNA-Seq reveals  
1371 unannotated transcripts and isoform switching during cell differentiation. *Nat*  
1372 *Biotech* **28**, 511-515 (2010).  
1373
- 1374 53. Logan-Klumpler FJ, *et al.* GeneDB--an annotation database for pathogens.  
1375 *Nucleic acids research* **40**, D98-108 (2012).  
1376
- 1377 54. Alexa A, Rahnenfuhrer J, Lengauer T. Improved scoring of functional groups  
1378 from gene expression data by decorrelating GO graph structure. *Bioinformatics*  
1379 **22**, 1600-1607 (2006).  
1380  
1381

# Figure 1. Pooled screens of an extensively characterized *pB*-mutant pilot-clone-library allow robust identification of heat-shock phenotypes

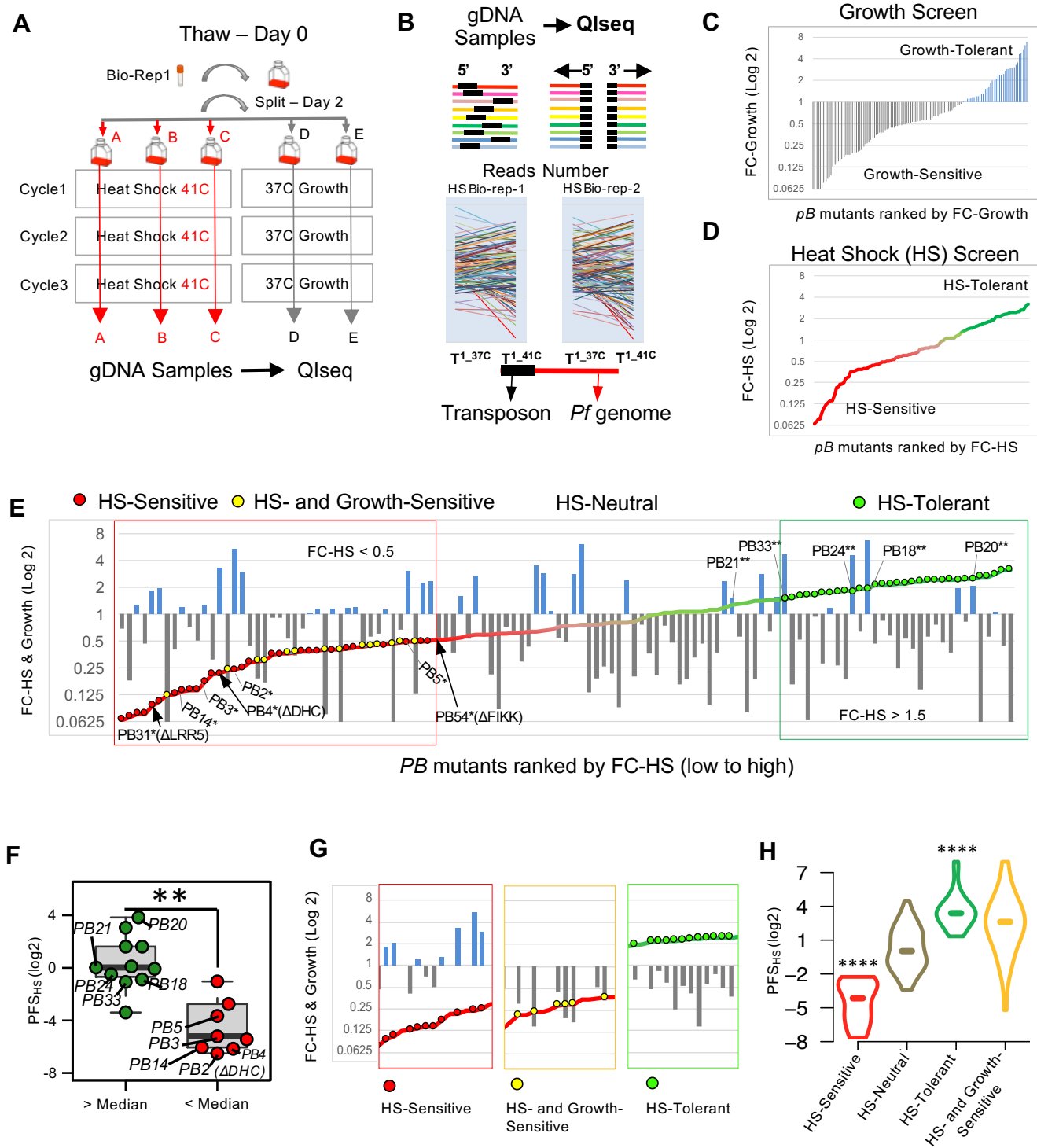


## Figure 2. Pooled phenotypic screens scaled up to a 1K-*pB*-mutant library enable identification of processes driving the *P. falciparum* heat-shock response

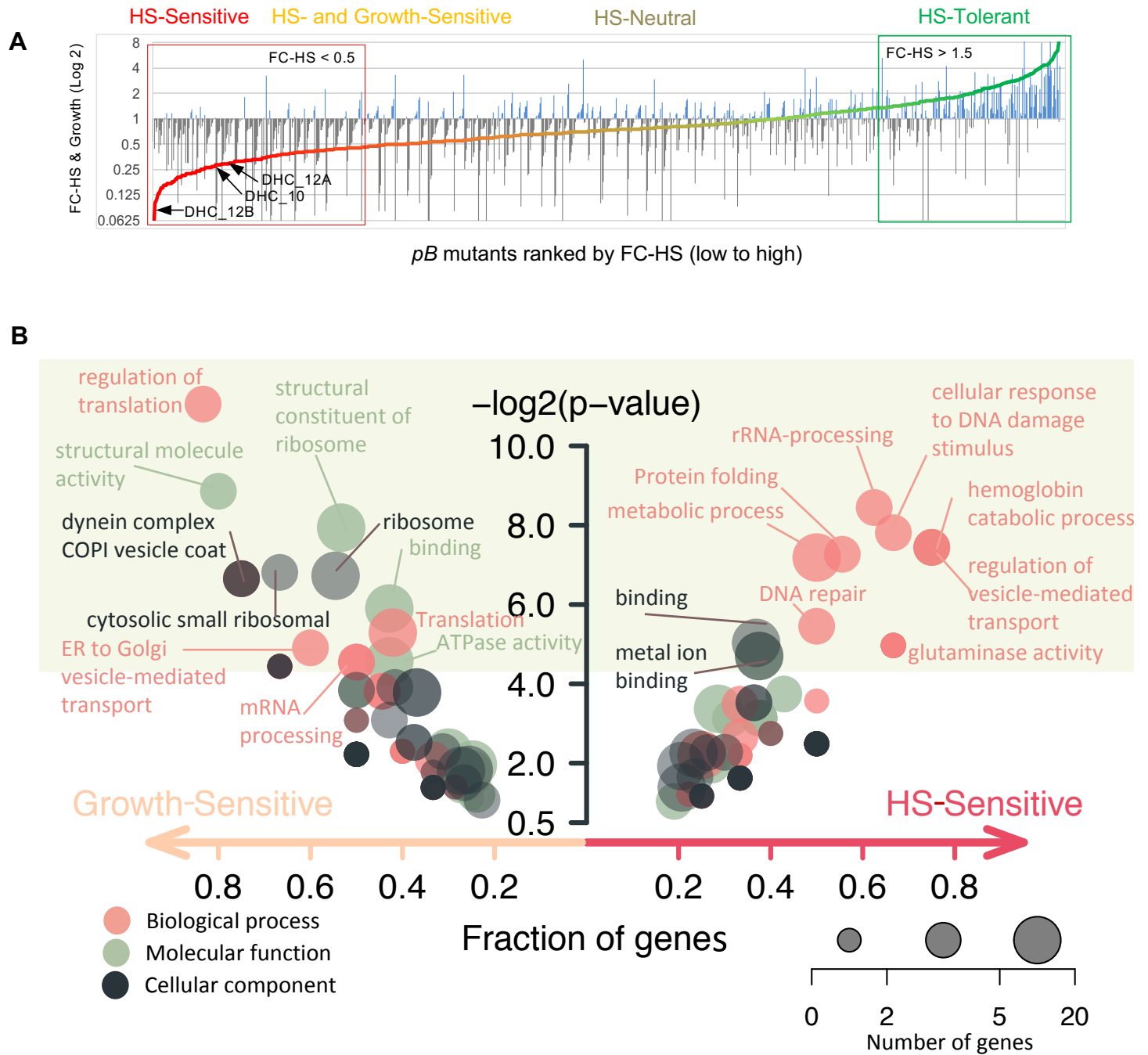


### Figure 3. Unfolded protein response, apicoplast-targeted and mitochondria-targeted stress-response pathways are critically dysregulated in functionally unrelated HS-sensitive mutant clones.

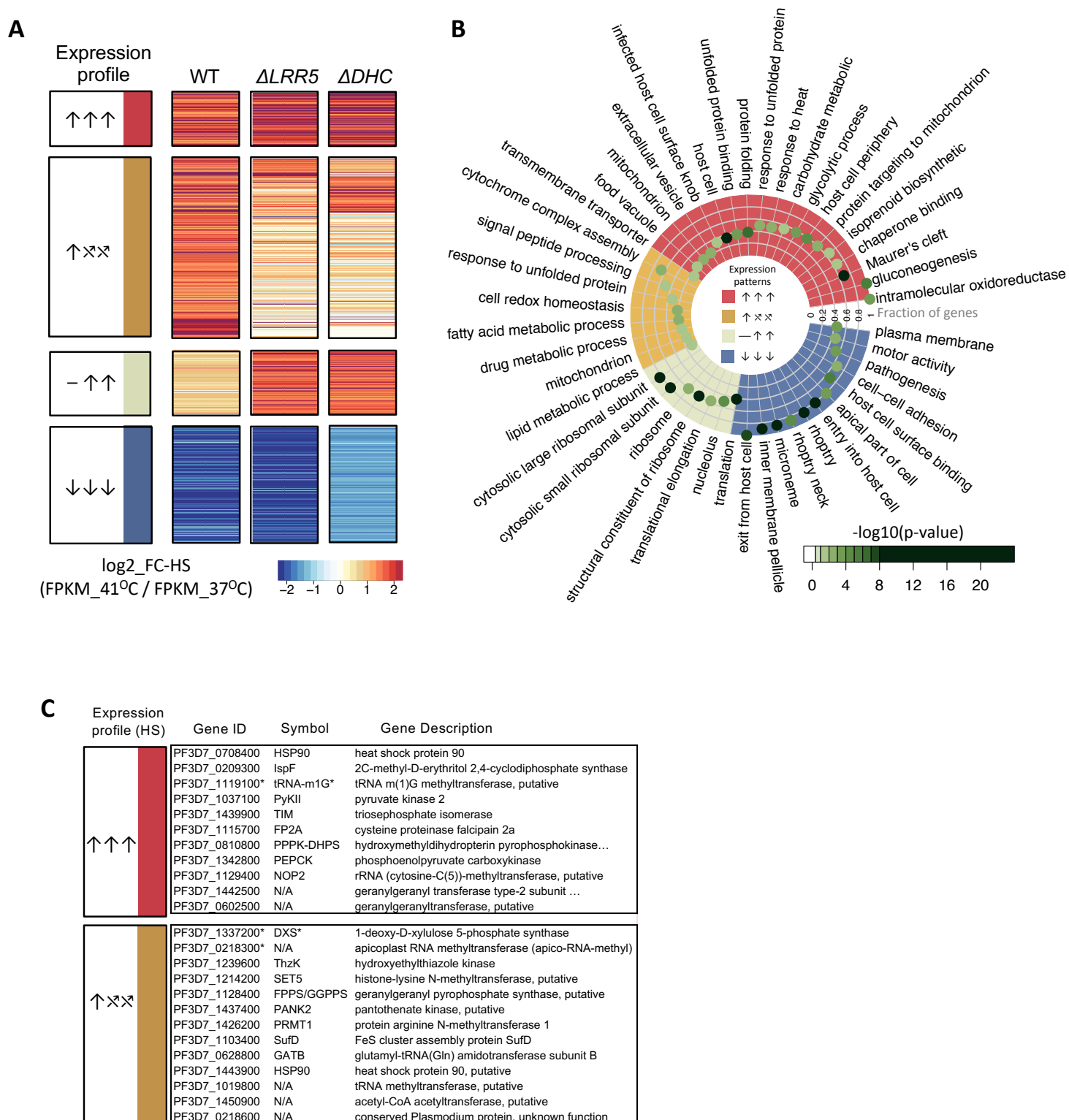


## Figure 4. Apicoplast isoprenoid biosynthesis is critical for *P. falciparum* survival of febrile temperatures

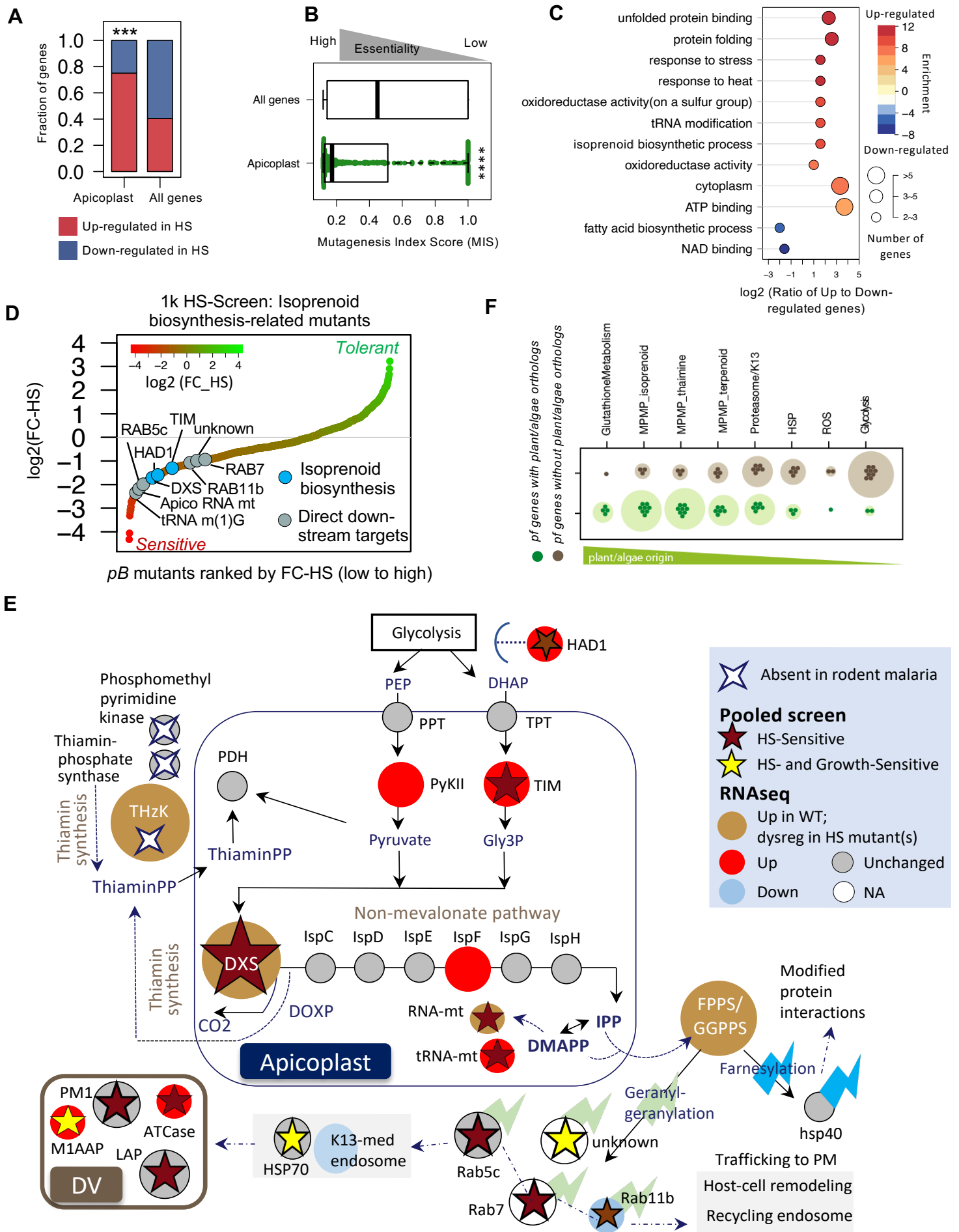


## Figure 5. Increased sensitivity to fever is directly correlated with increased sensitivity to artemisinin in the malaria parasite

